A DESIGN MODEL FOR FIBRE REINFORCED CONCRETE BEAMS PRE-STRESSED WITH STEEL AND FRP BARS

Joaquim A. O. Barros[1], Mahsa Taheri [2], Hamidreza Salehian[3], Pedro J. D. Mendes[4]

Abstract

This paper presents a design oriented model to determine the moment-curvature relationship of elements of rectangular cross section failing in bending, made by strain softening or strain hardening fibre reinforced concrete (FRC) and reinforced with perfectly bonded pre-stressed steel and fibre reinforced polymeric (FRP) bars. Since FRP bars are not affected by corrosion, they have the minimum FRC cover thickness that guaranty proper bond conditions, while steel bars are positioned with a thicker FRC cover to increase their protection against corrosion. Using the moment-curvature relationship predicted by the model in an algorithm based on the virtual work method, a numerical strategy is adopted to evaluate the load-deflection response of statically determinate beams. The predictive performance of the proposed formulation is assessed by simulating the response of available experimental results. By using this model, a parametric study is carried out in order to evaluate the influence of the main parameters that characterize the post cracking behaviour of FRC, and the pre-stress level applied to FRP and steel bars, on the moment-curvature and load-deflection responses of this type of structural elements. Finally the shear resistance of this structural system is predicted.

KEYWORDS: Fibre reinforced concrete; strain hardening; strain softening; flexural reinforcement; pre-stressed steel bars; pre-stressed FRP bars.

1. Introduction

The corrosion of steel bars reinforcement is the major cause of pathologies observed in reinforced concrete (RC) structures. The relatively small concrete cover of the steel reinforcement contributes for the initiation and development of this phenomenon, leading to a significant decrease of the load

[1] Full Professor, ISISE, Dept. of Civil Engineering, Univ. of Minho, Campus de Azurém, 4810-058 Guimarães, Portugal.
E-mail: barros@civil.uminho.pt; *Corresponding author*
[2] PhD Student, ISISE, Dept. of Civil Engineering, Univ. of Minho, Campus de Azurém, 4810-058 Guimarães, Portugal.
E-mail: taheri@civil.uminho.pt
[3] PhD Student, ISISE, Dept. of Civil Engineering, Univ. of Minho, Campus de Azurém, 4810-058 Guimarães, Portugal.
E-mail: salehian@civil.uminho.pt
[4] Researcher, ISISE, Dept. of Civil Engineering, Univ. of Minho, Campus de Azurém, 4810-058 Guimarães, Portugal.
E-mail: pmendes@civil.uminho.pt

carrying capacity of the member. The costs for the rehabilitation of corroded RC structures are, in certain cases, so high that a decision for demolition is relatively frequent, with the consequent economic, social and environmental adverse impacts.

The knowledge acquired at the level of the behaviour of fibre reinforced polymer (FRP) materials applied in the industry of Civil Construction has increased significantly in the last two decades. In fact, the possible substitution of conventional steel reinforcement by FRP bars has been investigated [1-3] to avoid corrosion problems and to improve the durability of concrete structures in adverse environmental conditions (marine, under-ground, and chemical industrial plants), and in thin structural elements. When compared to steel, the FRPs have higher resistance to corrosion, and higher strength-to-weight ratio. Furthermore, they are non-conductive for electricity and non-magnetic. However, the major obstacles of the application of FRP bars as a reinforcing material for concrete structures are the high initial costs, low modulus of elasticity, lack of ductility (linear stress-strain diagram up to rupture with no discernible yield point) and the small number of reliable design formulations to predict the behaviour of concrete elements reinforced internally with FRP bars [2, 4-8]. Concrete members reinforced with FRP subject to bending behave linearly up to cracking, and almost linearly after cracking with a lower flexural stiffness when compared with homologous beams reinforced with steel bars. Deflections and strains of concrete members reinforced with FRP bars are generally larger than of homologous members reinforced with steel bars. This is due to the low modulus of elasticity and the different bond characteristics of the FRP reinforcements [3, 9, 10]. In addition, as a result of larger crack width and smaller compressive stress block, the shear capacity of concrete beams is lower than when using high bond steel bars [7].

In an attempt of overcoming these drawbacks, some researchers [10-13] proposed a combination of FRP and steel reinforcements for concrete beams. Combining these reinforcement materials and considering the minor concrete cover required for FRP, an effective reinforcement solution in terms of durability is obtained by placing the FRP bars near the outer surface of the tensile zone, and steel bars at an inner level of the tensile zone (Fig. 1). The presence of steel bars in the above mentioned hybrid reinforcement system provides a significant contribution in terms of ductility and stiffness. The experimental tests where this hybrid reinforcement concept was used, in spite of being scarce, have confirmed the potentialities of this reinforcement system. For example, Tian and Yuan [10] concluded that the deflection of concrete beams reinforced simultaneously with GFRP (glass fibres) and steel bars was smaller than that of beams only reinforced with GFRP bars. Aiello and Ombres [11] verified that, in comparison with beams reinforced only with FRP bars, the participation of steel bars as part of the reinforcement system has reduced the crack width and crack spacing.

Pre-stressing the FRP bars can mobilize more effectively the strengthening potentialities of these reinforcing elements. Furthermore, by applying a certain pre-stress to the bars, a significant increase in terms of load carrying capacity can be obtained for deflection levels corresponding to the serviceability limit states. Applying steel and FRP bars with a certain pre-stress level can also contribute for the shear resistance of the element [11].

The research conducted in this paper is part of a research project aimed at developing high durable precast beams reinforced with a hybrid reinforcing system (pre-stressed steel and FRP bars), and adopting a high performance fibre reinforced concrete (HPFRC) to suppress the use of steel stirrups. According to this concept (Fig. 1), the steel reinforcement ratio should be designed in order to assure the safety of the structure in case of a fire occurrence and the consequent loss of FRP reinforcing capacities. The FRP and steel bars are applied with a certain pre-stress for the optimization of their reinforcing capabilities, to overcome the drawbacks derived from the relatively low elasticity modulus of FRP bars, and to increase the shear capacity of the beams. These beams can be used in multi-storey car parking, shopping centres, and residential and commercial buildings based on a precast constructive system. These beams can have a span between 6 and 11 meters.

Available research [15-19] evidences that steel fibres can substitute steel stirrups, especially when a high strength concrete is used and when beams are relatively shallow [17-18]. Steel fibres also reduce the width of shear cracks, thus also improving concrete durability [19]. In the study carried out by Meda et al. [19] the crack spacing in FRC beams was reduced in about 20 percent when compared to reference beams of conventional concrete with and without stirrups. Available research shows that up to a maximum crack width of 0.25 mm, steel fibres are not affected by corrosion [20, 21]. Furthermore, advances in the manufacture technology of synthetic fibres show that these non-corrodible fibres have high possibilities for the shear resistance of RC elements [22].

According to the structural concept proposed in the present work, the total and relative reinforcement ratio of steel and FRP bars, as well as the pre-stress level, should be selected in order to assure that at the beam's failure the steel has already yielded. Furthermore, the increase of load carrying capacity, mainly at serviceability limit states, the reduction of costs maintenance and the increase of life cycle should justify the relatively higher initial costs of the materials used in this

structural system. The pre-stress level to be applied to the flexural reinforcements, and the performance of the FRC, mainly its post-cracking residual strength, should be designed in order to avoid the formation of cracks in the top surface of the beam during the application of the pre-stress in the production process, and to prevent the occurrence of shear failure mode.

This paper proposes a design approach for rectangular cross section FRC beams reinforced with pre-stressed FRP and steel bars. After the model description, its predictive performance is appraised and a parametric study is carried out in order to evidence the influence of relevant parameters of the model on the load carrying capacity and ductility performance of FRC-hybrid reinforced simple supported pre-stressed beams. The proposed formulation is prepared to work with FRC that has tensile strain softening (SS-FRC) or tensile strain hardening (SH-FRC) behaviour [23]. Finally, the shear capacity of this structural system is predicted by using an adapted version of the formulation proposed by CEB-FIP Model Code 2010 [24].

2. Numerical strategy for the evaluation of the moment-curvature and force deflection of FRC-hybrid pre-stressed beams

2.1. Constitutive laws of materials under consideration

The stress-strain ($\sigma-\varepsilon$) response in compression considered for the FRC is based on the model proposed by Soranakom and Mobasher, represented in Fig. 2 [21]. As shown in Fig. 2a, the linear portion of an elastic–perfectly plastic compressive stress–strain response terminates at a "pseudo-yield" point $\left(\varepsilon_{cy},\sigma_{cy}\right)$ and remains constant with a compressive "yield" stress, σ_{cy}, until the ultimate compressive strain, ε_{cu}. To have the possibility of simulating FRCs that have distinct Young's modulus in compression and in tension (E_c and E, respectively), a normalized compressive stiffness factor (γ) is introduced as the ratio between E_c and E (Fig. 2a). As shown in Fig. 2b, the tensile behaviour is described by a tri-linear diagram with an elastic range defined by the tensile modulus E, followed by a post-cracking modulus (E_{cr}) that can be obtained by using a post-crack modulus parameter (η). By setting η to either a negative or a positive value, the same model can be used to simulate strain softening (SS) or strain hardening (SH) FRCs, respectively. At the third region of the tensile response, tensile stress $\left(\sigma_{cst}\right)$ remains constant up to the ultimate tensile strain $\left(\varepsilon_{tu}\right)$ that is a multiple of the cracking strain, e.g. $\varepsilon_{tu}=\beta_{tu}\,\varepsilon_{cr}$. Introducing the concept of residual strength

parameter, μ, the σ_{cst} can be defined as function of the stress at crack initiation, $\sigma_{cst} = \mu\sigma_{cr}$. In this model ω is the normalized compressive "yield" strain, and β_{tu} and λ_{cu} are the normalized ultimate tensile and compressive strain, respectively. The transition between the tensile softening/stiffening to the constant residual strength phase is defined by the α parameter, $\varepsilon_{tm} = \alpha\varepsilon_{cr}$.

The FRC cross section (Fig. 1), of width b and depth d, can be reinforced with steel and FRP bars, being $\rho_s = A_s / (bd_s)$ and $\rho_f = A_f / (bd_f)$ the reinforcement ratio of steel and FRP bars, respectively, where A_s and A_f are the cross sectional areas of steel and FRP bars, and $d_s = d - C_s$ and $d_f = d - C_f$ are the internal arms of steel and FRP bars, respectively, being C_s and C_f the concrete cover for the steel and FRP bars. As Fig. 3 illustrates, the tensile behaviour of the steel bars is simulated by a bilinear stress-strain diagram, with a linear-elastic branch up to the yield strain $\left(\varepsilon_{sy} = \zeta\varepsilon_{cr}\right)$, followed by a perfectly plastic branch ($\sigma_{sy} = E_s\varepsilon_{sy}$) up to the ultimate tensile strain ($\varepsilon_{su} = \psi_{su}\varepsilon_{cr}$), after which the steel tensile strength capacity is assumed null. The steel modulus of elasticity ($E_s = \gamma_s E_s$) is defined from the FRC tensile modulus of elasticity (E) by using the steel stiffness factor (γ_s).

Fig. 4 represents the stress-strain linear-elastic diagram for modelling the FRP tensile behaviour. When attaining the ultimate tensile strain ($\varepsilon_{fu} = \nu_{fu}\varepsilon_{cr}$) the FRP bar fails. Using the FRP tensile stiffness factor (γ_f), the modulus of elasticity of the FRP is defined from E ($E_f = \gamma_f E$).

2.2. Closed-formulation to determinate the moment-curvature response

The tensile and compressive stress relationships of the cross section components can be normalized by the FRC stress at crack initiation, σ_{cr} ($= E\varepsilon_{cr}$), according to the following equations:

$$\frac{\sigma_t(\beta)}{E\varepsilon_{cr}} = \begin{cases} \beta & 0 < \beta \le 1 \\ 1 + \eta(\beta - 1) & 1 < \beta \le \alpha \\ \mu & \alpha < \beta \le \beta_{tu} \\ 0 & \beta > \beta_{tu} \end{cases} \tag{1}$$

$$\frac{\sigma_c(\lambda)}{E\varepsilon_{cr}} = \begin{cases} \gamma\lambda & 0 < \lambda \le \omega \\ \gamma\omega & \omega < \lambda \le \lambda_{cu} \\ 0 & \lambda > \lambda_{cu} \end{cases} \tag{2}$$

$$\frac{\sigma_s(\psi)}{E\,\varepsilon_{cr}}=\begin{cases}\gamma_s\psi & 0<\psi\le\zeta\\ \gamma_s\zeta & \zeta<\psi\le\psi_{su}\\ 0 & \psi>\psi_{su}\end{cases} \tag{3}$$

$$\frac{\sigma_f(\nu)}{E\,\varepsilon_{cr}}=\begin{cases}\gamma_f\,\nu & 0<\nu\le\nu_{fu}\\ 0 & \nu>\nu_{fu}\end{cases} \tag{4}$$

where σ_t and σ_c is the tensile stress and the compressive stress in the FRC, respectively, and σ_s and σ_f are the tensile stresses in the steel and FRP bars. The other dimensionless parameters are obtained from the following equations (Figs. 2 to 4):

$$\alpha=\frac{\varepsilon_{trn}}{\varepsilon_{cr}}\,;\beta_{tu}=\frac{\varepsilon_{tu}}{\varepsilon_{cr}}\,;\eta=\frac{E_{cr}}{E}\,;\mu=\frac{\sigma_{cst}}{E\,\varepsilon_{cr}} \tag{5}$$

$$\gamma=\frac{E_c}{E}\,;\ \omega=\frac{\varepsilon_{cy}}{\varepsilon_{cr}}\,;\lambda_{cu}=\frac{\varepsilon_{cu}}{\varepsilon_{cr}} \tag{6}$$

$$\gamma_s=\frac{E_s}{E}\,;\ \zeta=\frac{\varepsilon_{sy}}{\varepsilon_{cr}}\,;\ \psi_{su}=\frac{\varepsilon_{su}}{\varepsilon_{cr}} \tag{7}$$

$$\gamma_f=\frac{E_f}{E}\,;\ \nu_{fu}=\frac{\varepsilon_{fu}}{\varepsilon_{cr}} \tag{8}$$

The normalized tensile strain at the concrete bottom fibre (β), the normalized compressive strain at the concrete top fibre (λ), and the normalized tensile strain of the steel (ψ) and FRP (ν) are defined as:

$$\beta=\frac{\varepsilon_{tbot}}{\varepsilon_{cr}}\,;\ \lambda=\frac{\varepsilon_{ctop}}{\varepsilon_{cr}}\,;\ \psi=\frac{\varepsilon_s}{\varepsilon_{cr}}\,;\ \nu=\frac{\varepsilon_f}{\varepsilon_{cr}} \tag{9}$$

A linear variation of strain can be assumed on the depth of the section and, hence β, λ, ψ and ν parameters are linearly related together:

$$\lambda=\frac{k}{1-k}\beta \tag{10}$$

$$\psi=\frac{1-k-\Delta_s}{1-k}\beta \tag{11}$$

$$\nu=\frac{1-k-\Delta_f}{1-k}\beta \tag{12}$$

where k, Δ_s and Δ_f are the neutral axis depth ratio, and the normalized central distance of steel and FRP bars from tensile face of section, respectively (Fig. 1).

To apply a certain pre-stress level to both steel and FRP bars (assuming perfect bond to FRC), two independent initial tensile strains are considered, designated by steel pre-stressing strain, ε_s^{pr} , and FRP pre-stressing strain, ε_f^{pr} , respectively. The pre-stress level for the steel and FRP bars is defined as the ratio between ε_s^{pr} and the steel tensile yield strain (ε_{sy}), and the ratio between ε_f^{pr} and the FRP ultimate tensile strain $\left(\varepsilon_{fu}\right)$, respectively. Assuming the variation of pre-stress levels in the range [0-1], pre-stressed strains are restricted to the linear elastic region of steel and FRP tensile stress-strain response (Figs. 3 and 4). The pre-stress level depends on the type of FRP bars and loading conditions, and should be in agreement with the recommendations of [5-8]. Therefore, the pre-stress loads for the steel (F_s^{pr}) and FRP (F_f^{pr}) are obtained from the following equations:

$$F_s^{pr} = \varepsilon_s^{pr} \gamma_s E \rho_s b d_s \tag{13}$$

$$F_f^{pr} = \varepsilon_f^{pr} \gamma_f E \rho_f b d_f \tag{14}$$

Regarding to the depth of the neutral axis (kd), the bending moments corresponding to pre-stress loads are calculated by the following equations:

$$M_s^{pr} = F_s^{pr} (1 - k - \Delta_s) d \tag{15}$$

$$M_f^{pr} = F_f^{pr} (1 - k - \Delta_f) d \tag{16}$$

To calculate the moment-curvature ($M - \chi$) diagram, it is assumed that a plane section remains plane after bending, and shear deformation of the section can be ignored. A gradual increment is applied to the normalized tensile strain at the concrete bottom fibre (β), and corresponding values of the normalized compressive strain at the concrete top fibre (λ), and the normalized tensile strain of the steel (ψ) and FRP (ν) are obtained from Eqs. (10) to (12).

Due to the specificities of the constitutive laws of the intervening materials, the nine strain configurations indicated in Table 1 need to be considered [26]. There are three possible main configurations for tensile strain at bottom fibre (Table 1): $0 < \beta \le 1$, $1 < \beta \le \alpha$, and $\alpha < \beta \le \beta_{tu}$. Each configuration 2 and 3 (see Table 1) has four possible conditions due to the value of concrete compressive strain at top fibre in either elastic ($0 < \lambda \le \omega$) or plastic ($\omega < \lambda \le \lambda_{cu}$) behaviour in compression, and regarding the value of steel tensile strain in either elastic $\left(0 < \psi \le \zeta\right)$ or plastic ($\zeta < \psi \le \psi_{su}$) behaviour, and also due to the value of FRP tensile strain $\left(0 < \nu \le \nu_{fu}\right)$.

For each strain configuration the value of k parameter can be obtained by the equations presented in Table 2 [26]. After obtaining the k value in each strain configuration, internal moment is calculated by operating on the force components and their distance from neutral axis. The corresponding curvature is also determined as the ratio between the concrete compressive strain at top fibre of the cross section and the depth of the neutral axis. The moment and curvature at stage i of the loading process (M_i, χ_i) is obtained from the following equations:

$$M_i = M_i' M_{cr} \tag{17}$$

$$\chi_i = \chi'_i \ \chi_{cr} \tag{18}$$

where M_i' and χ'_i are the normalized moment and curvature at stage i obtained from Table 3 [26]. In equations (17) and (18) M_{cr} and χ_{cr} are the cracking moment and the corresponding curvature, respectively, calculated for a rectangular cross section from the following equations:

$$M_{cr} = \frac{1}{6} b d^2 \left(E \varepsilon_{cr}\right) \tag{19}$$

$$\chi_{cr} = \frac{2\varepsilon_{cr}}{d} \tag{20}$$

2.3. Model to estimate the force-deflection relationship

The force-deflection response of a statically determinate beam failing in bending is determined by the algorithm schematically represented in Figure 5. According to this approach, for successive χ_i of the $M-\chi$ relationship of the beam mid-span section the corresponding M_i is read, and the total applied load P_i is determined by equilibrium of the beam, as well as the beam bending diagram M_i. Decomposing the beam in small segments, the bending moment in a generic cross section at a distance x can be determined, $M_i(x)$, and from the $M-\chi$ relationship of this cross section, the corresponding flexural stiffness $EI_i(x)$ is obtained, as well as the bending moment in this section for the base system corresponding to the evaluation of the deflection at the beam mid-span, $\bar{M}(x)$. By applying the Virtual Work Method, the mid-span deflection of the beam for the i^{th} loading step, $\left(\delta_{mid}\right)_i$, is determined, which, together with P_i provides a point of the P-δ curve.

3. Model appraisal

To evaluate the accuracy of the proposed model, the results of the software developed according to the described algorithm were compared to the results obtained from DOCROS software [27]. The model implemented in DOCROS assumes that a plane section remains plane after deformation and bond between materials is perfect. The section is divided in layers, and the thickness and width of each layer is user-defined and depend on the cross-section geometry. DOCROS can analyze sections of irregular shape and size, composed of different types of materials subjected to an axial force and variable curvature. DOCROS has a wide database of constitutive laws for the simulation of monotonic and cyclic behaviour of cement based materials, polymer based materials and steel bars.

The predictive performance of the model was assessed by evaluating the moment-curvature relationship for a rectangular cross section of 250 mm width and 500 mm depth, of a beam reinforced longitudinally with a percentage of steel bars of 0.2 and a percentage of FRP bars of 0.1. FRP bars have a concrete cover of 30 mm, while steel bars are positioned deeper, at a distance of 80 mm from tensile face of the section. Furthermore, a pre-stress percentage of 50% was applied to both, steel and FRP bars. The values of the model parameters are included in Table 4.

Moment-curvature relationships predicted by the proposed model and those obtained from DOCROS software are compared in Figures 6a and 6b for cross section of beams made by strain softening and strain hardening FRC, respectively, revealing the high accuracy of the developed model.

The predictive performance of the model was also evaluated by simulating experimental tests with FRP strengthened RC beams, carried out by Badawi and Soudki [28], and by Xue *et al.* [29]. As Fig. 7 shows, two different strengthening techniques were adopted: the first one applying a pre-stressed longitudinal GFRP bar (glass fibres reinforced polymer) placed into a groove open on the concrete cover of the beam, in agreement with the procedures of the near surface mounted (NSM) technique [28]; and the second one applying a pre-stressed CFRP laminate (carbon fibre reinforced polymer) according to the externally bonded reinforcement (EBR) technique [29]. The data to define the geometry, the reinforcement and the strengthening arrangements ~~is~~ are included in Tables 5 and 6, while Table 7 presents the relevant values of the parameters that define the constitutive laws of the intervening materials. Since non-fibrous concrete was used in these RC beams, the contribution of the

post-cracking residual strength of this material for the flexural resistance of these beams was neglected (μ=0). Fig. 8 compares the load-deflection responses predicted by the proposed formulation and those recorded in the tests, which evidences the capability of the model to predict with good accuracy the deflection response of this type of structural elements.

4. Parametric studies

To assess the influence of the relevant mechanical properties of FRC, and the pre-stress level applied to FRP and steel bars, on the moment-curvature relationship and on the force-deflection of hybrid reinforced FRC beams, a parametric study was carried out adopting a simply supported beam with the geometry, the reinforcement arrangement and the loading conditions represented in Fig. 9. Three distinct pre-stress levels were considered, 0% (non pre-stressed), 25%, and 50%, which is a percentage of the yield stress of the steel bars and a percentage of the tensile strength of the FRP bars. However, due to the susceptibility to creep rupture of some types of FRP bars (mainly those made by glass fibres, GFRP), the limits recommended by some standards [5-8] for the stress limits in these reinforcements under sustained stresses should be considered. If FRP bars are subjected to cyclic or fatigue loading, the stress limits proposed by these standards should be also taken into account.

For the influence of the FRC post-cracking performance, the values of 0.0, 0.4, 0.8, and 1.2 for the normalized residual strength (μ) were adopted, maintaining constant the normalized transition strain of α=10.0. In this context, the influence of the α parameter was also assessed by adopting values of 1.01, 10, 50, and 150, keeping constant the normalized residual strength (μ=0.4). For the parametric study, the values of the parameters that define the constitutive laws of the intervening materials are indicated in Table 8. For this parametric study GFRP bars were considered.

The moment-curvature and the load-deflection curves corresponding to this parametric study are presented in Figs. 10 to 15. As expected, for the considered statically determinate beam the variation of load-deflection follows the variation of the corresponding moment-curvature.

4.1. Influence of α parameter and pre-stress level on the moment-curvature and load-deflection responses of hybrid reinforced FRC beams

For each adopted pre-stress level of FRP and steel bars, the influence of α FRC-related parameter in terms of moment-curvature and load-deflection responses is represented in Figures 10a-c and 10d-f, respectively. The points corresponding to the concrete crack initiation and the steel yield initiation are also signalized in the curves of Fig. 10. Since α is as a post cracking parameter of FRC, it has no effect in the responses before crack initiation. However, after crack initiation the flexural capacity of the cross section and the load carrying capacity of the beam are significantly increased with the increase of α parameter. In fact, the moment and the load at yield initiation of steel bars increase with α, and this tendency is also observed for the corresponding curvatures and deflections. Therefore, the residual strength of FRC between ε_{cr} and $\varepsilon_{trn} = \alpha\varepsilon_{cr}$ (see Fig. 2a) has a significant favourable impact on the flexural and load carrying capacities corresponding to the level of curvatures and deflections installed in this type of structural elements at serviceability limit states.

According to Fig. 10, the moment-curvature and load-deflection diagrams corresponding to the lowest adopted values of normalized transition strain (α=1.01 and α=10) are only different in a relatively small amplitude of curvature and deflection just after crack initiation. This difference, that is more significant in terms of load-deflection, is a consequence of the post-cracking residual strength of the concrete between ε_{cr} and $\varepsilon_{trn} = \alpha\varepsilon_{cr} = 10\,\varepsilon_{cr}$ when $\alpha = 10$. Furthermore, the increase of α parameter from 10 to 150 provides significant improvement of those responses. For the deflection corresponding to the serviceability limit state conditions ($\delta = L_s$ /250=2500/250=10 mm [14]), the increase percentage in the load carrying capacity ($\Delta P_{\delta=10mm} / P^{\alpha=1.01}_{\delta=10mm}$, where $P^{\alpha=1.01}_{\delta=10mm}$ is the load at δ=10mm for α=1.01) by adopting the α values of 10, 50 and 150 is 8%, 35% and 47% for pr=0%; 4%, 20% and 27% for pr=25%; and 3%, 14% and 19% for pr=50%. Due to the linear behaviour of FRP bars, the moment-curvature and the load-deflection diagrams vary almost linearly between steel yield point and ultimate condition (all the analysis were interrupted when the tensile strength of FRP was attained).

The influence of the pre-stress percentage on the moment-curvature and load-deflection responses is illustrated in Figures 11a-d and 12a-d, respectively, for the different values of α considered. As expected, for a given α value, the moment and the load at crack initiation has increased with the

applied pre-stress, but the moment and the load at yield initiation of the steel bars was not significantly affected by the pre-stress level. However, due to the initial tensile strain introduced in the steel bars when pre-stress is applied, the curvature and the deflection at yield initiation decrease with the increase of the pre-stress level, and this is more pronounced with the increase of the pre-stress level. Due to similar reason, the curvature and the deflection at the rupture of the FRP bars decrease with the increase of the pre-stress level applied to these bars. Figs. 11e-h show that the $\Delta M = M^{pr=25/50} - M^{pr=0.0}$ increases with the pre-stress level, being $M^{pr=25/50}$ the moment for a pre-stress level of 25% or 50%, and $M^{pr=0.0}$ the moment for non pre-stressed beam. However, the maximum increase of ΔM is almost the same regardless the value of α considered. Similar tendency is observed for the increase of $\Delta P = P^{pr=25/50} - P^{pr=0.0}$ with the pre-stress level (Fig. 12e-h).

Figs. 11a-d and 12a-d also show that the curvature and the deflection at steel yield initiation decrease with the increase of the pre-stress level applied to steel and FRP bars, while the deflection at crack initiation is not affected significantly. Therefore, the deflection amplitude between crack initiation and steel yield initiation decreases with the increase of the pre-stress level, reducing the ductility of the response of the beams. However, a hybrid reinforced FRC beam can be designed in order that the maximum ΔP occurs at a deflection level larger than the deflection at serviceability limit states (with an amplitude decided by the designer), as is the case of the present analysis.

4.2. Influence of μ parameter and pre-stress level on moment-curvature and load-deflection responses of hybrid reinforced FRC beams

Figures 13a-c and 13d-f represent the influence of normalized residual strength, μ , in terms of moment-curvature and load deflection responses, respectively. The increase of this parameter provides a significant increase of the flexural strength and load carrying capacity. In fact, for the deflection corresponding to the serviceability limit states conditions (δ=10 mm) the $\Delta P_{\delta=10mm} / P_{\delta=10mm}^{\mu=0.0}$ (where $P_{\delta=10\,mm}^{\mu=0.0}$ is the load at δ=10mm for μ=0.0) for μ values of 0.4, 0.8 and 1.2 is 31%, 68% and 1037% for pr=0%; 20%, 41% and 61% for pr=25%; and 14%, 29% and 42% for pr=50%. The increase level in terms of flexural strength and load carrying capacity provided by the increase of μ remains almost constant up to the rupture of the FRP (the occurred failure condition). The moment at yield

initiation of steel bars and its corresponding curvature increase with μ. The same tendency occurs in the load carrying capacity at yield initiation of steel bars. The increase of μ has also a favourable effect on increasing the deflection corresponding to the load at yield initiation of steel bars when the pre-stress level increases.

The influence of the pre-stress percentage on the moment-curvature and load-deflection responses is illustrated in Figures 14a-d and 15a-d, respectively, for the different values of μ considered. As expected, for a given μ value, the moment and the load at crack initiation increase with the applied pre-stress, but the moment and the load at yield initiation of the steel bars were not significantly affected by the pre-stress level. The difference between the curvatures at yield and crack initiation decreases with the increase of the pre-stress level, which also occurs in the load-deflection response, indicating a decrease of the ductility performance of the beam. As expected, the curvature and the deflection at failure of the FRP also decrease with the increase of the pre-stress level.

Figs. 14e-h show that the $\Delta M = M^{pr=25/50} - M^{pr=0.0}$ increases with the pre-stress level. However, the maximum increase of ΔM is almost the same regardless the value of μ considered. Similar tendency is observed for the increase of $\Delta P = P^{pr=25/50} - P^{pr=0.0}$ with the pre-stress level (Fig. 15e-h).

5. Shear resistance

The load carrying capacity of a FRC beam flexurally reinforced with pre-stressed steel and FRP bars can be limited by its shear resistance. To predict the shear resistance of this new structural system, the recommendations of the CEB-FIP Model Code 2010 [24] are adopted. According to this document, the shear resistance of a FRC beam that has longitudinal reinforcement can be determined from the following equation:

$$V_{Rd} = V_{Rd,s} + V_{Rd,F} \leq V_{Rd,\max} \tag{21}$$

where the equations for the evaluation of the contribution of the steel stirrups and to avoid crushing of the compression struts are indicated in the prEN 1992-1-1 [30]. The term $V_{Rd,F}$ represents the contribution of the FRC for the shear resistance, and is obtained from equation:

$$V_{Rd,F} = \left\{ \frac{0.18}{\gamma_c} \cdot k_d \cdot \left[100 \cdot \rho_1 \cdot \left(1 + 7.5 \cdot \frac{f_{Ftuk}}{f_{ctk}} \right) \cdot f_{ck} \right]^{1/3} + 0.15 \cdot \sigma_{cp} \right\} \cdot b_w \cdot d \qquad (22)$$

where [24]:

γ_c is the partial safety factor for the concrete (1.5);

k_d is a factor that takes into account the size effect and is equal to:

$1 + \sqrt{\frac{200}{d}} \leq 2.0$ with d being the effective depth of the cross section in mm;

ρ_l is the reinforcement ratio of the longitudinal reinforcement, equal to

$\rho_l = A_{sl} / b_w d$, being the A_{sl} [mm^2] the cross sectional area of the reinforcement which extends $l_{bd}+d$ beyond the considered section (l_{bd} is the design anchorage length [mm]), and b_w [mm] is the smallest width of the cross-section in the tensile area;

f_{ctk} [MPa] is the characteristic value of the tensile strength for the concrete matrix;

f_{ck} [MPa] is the characteristic value of cylindrical compressive strength for the concrete matrix;

σ_{cp} [MPa] $= N_{Ed}/A_c < 0.2\ f_{cd}$ [MPa] is the average stress acting on the concrete cross section, A_c [mm^2], for an axial force N_{Ed} [N], due to loading or pre-stressing actions ($N_{Ed} > 0$ for compression), and f_{cd} is the design value of the concrete compressive strength;

f_{Ftuk} [MPa] is the characteristic value of the ultimate residual tensile strength of FRC, that can be determined following the recommendations of [24].

To adapt equation (22) for the case of a hybrid reinforced beam, ρ_l is replaced by the equivalent steel reinforcement ratio:

$$\rho_{s,eq} = \frac{A_s}{bd_s} + \frac{E_f}{E_s}\frac{A_f}{bd_f} \tag{23}$$

and d is substituted by the equivalent steel effective depth

$$d_{s,eq} = \frac{A_s\, d_s + \left(E_f / E_s\right) A_f\, d_f}{A_s + \left(E_f / E_s\right) A_f} \tag{24}$$

where the meaning of the symbols were already introduced. Since in the parametric studies, design values were assumed for the parameters that define the constitutive laws of the materials, in the present approach it is considered that $f_{Ftuk} = \gamma_F \ (\mu\sigma_{cr})$, where γ_F =1.5 is the partial safety factor recommended by the Model Code [24] for FRC. Considering the beam of Fig. 9 adopted in the parametric studies, and the properties of Table 8, by fixing α =10 and varying the pre-stress level applied to the steel and FRP bars, and ranging the μ according to the values indicated in this table, the load carrying capacity of the beams limited by the shear (P_{sh}=2×V_{Rd}) and flexural resistance (P_{fl}) are compared in Table 9. In this study, P_{fl} is the load when the minimum strain between $\varepsilon_{cu} = \lambda_{cu}\,\varepsilon_{cr}$ (concrete crushing) $\varepsilon_{su} = \psi_{su}\,\varepsilon_{cr}$ (steel rupture) and $\varepsilon_{fu} = \nu_{fu}\,\varepsilon_{cr}$ (FRP rupture) is attained. From the obtained results it can be concluded that shear failure only occur in non-fibrous concrete beams when the pre-stress level is lower than 50%. When f_{Ftuk} is higher than 40% of the characteristic value of the stress at crack initiation, $0.4\,f_{ctk}$, flexural failure mode is always guaranteed for the analyzed beams.

However, since the CEB-FIP Model Code formulation was developed by considering, mainly, the data available for steel fibre reinforced concrete beams flexurally reinforced with passive steel bars, the use of Equation (22) for FRC hybrid pre-stressed beams should be used with caution. In fact, according to the knowledge of the authors the predictive performance of Equation (22) for this type of beams was not yet assessed because experimental data is not available.

6. Conclusions

In this work a design oriented model was proposed for determining the moment-curvature response of rectangular cross section of FRC members reinforced by longitudinal pre-stressed steel and FRP bars that fail in bending. By using a trilinear stress-strain diagram for the tensile behaviour of FRC, the proposed model is capable of simulating both strain softening and strain hardening FRC materials. A relatively small number of parameters is necessary to characterize the FRC behaviour in tension and in compression, as well as the behaviour of steel and FRP bars in tension. Using the moment-curvature relationship predicted by the model and implementing an algorithm based on the virtual work method, a numerical strategy was developed for the prediction of the force-deflection response of statically determinate beams. The good predictive performance of the model was assessed by simulating the force-deflection responses registered in experimental programs. The model is capable of simulating the behaviour of beams internally reinforced with steel and FRP bars, and can also be used to predict the force-deflection relationship of RC beams flexurally strengthened with pre-stressed FRP systems applied according to the near surface mounted (NSM) and externally bonded reinforcement (EBR) techniques.

The proposed methodology was used to execute a parametric study to evaluate the influence of the following parameters on the moment-curvature and force-deflection responses: $\alpha = \varepsilon_{trn}/\varepsilon_{cr}$ and μ (normalized residual strength) FRC-related parameters and pre-stress level. From this parametric study the following main observations can be pointed out:

- The flexural capacity of the cross section and the load carrying capacity of the beam increase significantly with the increase of μ and α parameters;

- The moment at yield initiation of steel bars and its corresponding curvature increase with μ and α . The same tendency occurs for the load carrying capacity at yield initiation of steel bars;

- The increase of μ and α has also the favourable effect of increasing the deflection corresponding to the load at yield initiation of steel bars when the pre-stress level increases;

- For the deflection corresponding to the serviceability limit states conditions, the increase of μ and α leads to a significant increase of the load carrying capacity;

- By increasing the pre-stress level in the steel and FRP bars, the curvature and the deflection at steel yield initiation, as well the curvature and the deflection at failure decrease. Therefore, since the deflection at crack initiation is not affected significantly by the applied pre-stress level, the deflection amplitude between crack initiation and steel yield initiation decreases with the increase of the pre-stress level, reducing the ductility of the response of the beams. However, the FRC can be optimized in order to provide values for the μ and α parameters that guarantee the aimed degree of ductility when applying a certain pre-stress level in a hybrid reinforced beam.

- For the beams considered in the parametric studies, shear failure never occur if FRC with $\mu \geq 0.4$ is adopted, regardless the pre-stress level applied to the longitudinal bars.

7. Acknowledgements

The study reported in this paper is part of the research program "DURCOST - Innovation in reinforcing systems for sustainable pre-fabricated structures of higher durability and enhanced structural performance" supported by FCT, PTDC/ECM/105700/2008. The second and forth authors acknowledge the research grant under the project QREN number 3456 "PONTALUMIS", while the third author acknowledges the support provided by FCT grant SFRH/BD/71934/2010.

8. References

[1] Thériault M, Benmokrane B. Effects of FRP Reinforcement Ratio and Concrete Strength on Flexural Behaviour of Concrete Beams. Journal of Composites for Construction 1998; 2(1): 7-16.

[2] Toutanji HA, Saafi M. Flexural Behaviour of Concrete Beams Reinforced with Glass Fibre-Reinforced Polymer (GFRP) Bars. ACI Structural Journal 2000; 97(5): 712-719.

[3] Abdalla HA. Evaluation of Deflection in Concrete Members Reinforced with Fibre Reinforced Polymer (FRP) Bars. Composite Structures 2002; 56: 63-71.

[4] Alsayed SH, Al-Salloum YA, Almusallam TH. Performance of Glass Fibre Reinforced Plastic Bars as a Reinforcing Material for Concrete Structures. Composites: Part B 2000; 31: 555-567.

[5] ACI 440R-07. Report on Fibre-Reinforced Polymer (FRP) Reinforcement for Concrete Structures. American Concrete Institute Reported by ACI Committee 440 2007: 100 pages.

[6] ACI 440.1R-06. Guide for the Design and Construction of Concrete Reinforced with FRP Bars. ACI 440.1R-06, American Concrete Institute Reported by ACI Committee 440 2007.

[7] CAN/CSA-S806-02. Design and Construction of Building Components with Fibre-Reinforced Polymers. Canadian Standards Association, Toronto, Ontario, Canada, (2007), 218p.

[8] CEB-FIP. FRP reinforcement in RC structures. Technical report on the Design and use of fibre reinforced polymer reinforcement (FRP) in reinforced concrete structures, prepared by a working party of the Task Group 9.3 2007: 175 pages.

[9] Bakis, C.E., Bank, L.C., Brown, V.L., Cosenza, E., Davalos, J.F., Lesko, J.J., Machida, A., Riskalla, S.H. and Triantafillou, T.C., 2002, "Fibre-Reinforced Polymer Composites for Construction – State-of-the-Art Review", Journal of Composites for Construction, vol. 6, n°2, May, pp. 73-87.

[10] Tian Y, Yuan Y. Deflection Prediction of Concrete Beams Reinforced with GFRP and Steel Rods. Proceedings (CD-ROM) of 8th International Symposium on Fibre Reinforced Polymer (FRP) Reinforcement for Concrete Structures (FRPRCS-8), Patras, 16-18 July 2007.

[11] Aiello MA, Ombres L. Structural Performances of Concrete Beams with Hybrid (Fibre-Reinforced Polymer-Steel) Reinforcements. Journal of Composites for Construction 2002; 6(2): 133-140.

[12] Leung HY, Balendran RV. Flexural Behaviour of Concrete Beams Internally Reinforced with GFRP Rods and Steel Rebars. Structural Survey 2003; 21(4): 146-157.

[13] Bischoff PH, Scanlon, A. Effective Moment of Inertia for Calculating Deflection of Concrete Members Containing Steel Reinforcement and Fiber-Reinforced Polymer Reinforcement. ACI Structural Journal, 104(1), 68-75, January-February 2007.

[14] prEN 1992-1-1; Eurocode 2: Design of concrete structures; Part 1-1: General rules and rules for buildings. 2010.

[15] Santos PFS, Barros JAO, Lourenço LAP. Steel fibres for the shear resistance of high strength concrete beams. Proceedings of 7th RILEM International Symposium on Fibre Reinforced Concrete Design and Applications (BEFIB 2008), Paper SIM01, Chennai, India, 17-19 September 2008.

[16] Barros JAO, Gettu R, Barragan BE. Material Nonlinear analysis of steel fibre reinforced concrete beams failing in shear. Proceedings of 6th International RILEM Symposium on fibre reinforced concrete (BEFIB 2004), Verona, Italy, 20-22 September 2004. p. 711-720.

[17] Casanova P. Bétons de fibres métalliques: du materiau à la structure. PhD Thesis. École Nationale des Ponts et Chaussées, Paris ; 1995. (in French)

[18] Casanova P, Rossi P, Schaller I. Can steel fibres replace transverse reinforcement in reinforced concrete beams? ACI Material Journal 2000; 94: 341-354.

[19] Meda A, Minelli F, Plizzari GP, Riva P. Shear behaviour of steel fibre reinforced concrete beams. Materials and Structures Journal 2005; 38: 343-353.

[20] Bernard ES. Durability of Fibre-Reinforced Shotcrete. Shotcrete: More Engineering Developments, Taylor and Francis, 2004: 59-64.

[21] Nemegeer D, Vanbrabant J, Stang H. Brite-Euram Program on Steel Fibre Concrete, Durability Corrosion Resistance of Cracked Fibre-Reinforced Concrete. In: Schnütgen B, Vandewalle L, editors. Test and Design Methods for Steel Fibre Reinforced Concrete-Background and Experiences. RILEM Technical Committee 162, TDF Workshop, Proceedings Pro 31, 2003: 47-66.

[22] Furlan S, Hanai JB. Shear behaviour of fibre reinforced concrete beams. Cement and Concrete Composites 1998; 19(4): 359-366.

[23] Naaman A. High performance fibre reinforced cement composites. In: Shi C, Mo Y. High-performance construction materials (Science and Application). World Scientific Publishing Co. Pte. Ltd, 2008 .

[24] Model Code 2010, Final draft, CEB-FIP, 2011.

[25] Soranakom C, Mobasher B. Correlation of tensile and flexural response of strain softening and strain hardening cement composites. Cement & Concrete Composites 2008; 30: 465-477.

[26] Taheri M, Barros JAO, Salehian H, A design model for fibre reinforced concrete elements reinforced by longitudinal prestressed steel and FRP bars failing in bending. Technical report 11-DEC/E-18, Department of Civil Engineering, University of Minho. June 2011, pp. 59.

[27] Basto CAA, Barros JAO. Numeric simulation of sections submitted to bending. Technical report 08-DEC/E-46, Department of Civil Engineering, University of Minho, August 2008, pp. 73.

[28] Badawi M, Soudki K. Flexural strengthening of RC beams with prestressed NSM CFRP rods – Experimental and analytical investigation. Journal of Construction and Building Materials 2009; 23: 3292-3300.

[29] Xue W, Tan Y, Zeng L. Flexural response predictions of reinforced concrete beams strengthened with prestressed CFRP plates. Journal of Composite Structures 2010; 92: 612–622.

[30] prEN 1992-1-1 - Eurocode 2: Design of concrete structures - Part 1-1: General rules and rules for buildings, 2010.

Notation

A_c	=	the concrete cross section
A_f	=	cross sectional area of FRP bar
A_s	=	cross sectional area of steel bar
A_{sl}	=	cross sectional area of the reinforcement
b	=	beam width
b_w	=	smallest width of the cross-section in the tensile area
C_s	=	central distance of steel bars from tensile face of section
C_f	=	central distance of FRP bars from tensile face of section
d	=	effective depth of beam
d_s	=	central distance of steel bars from top face of section
$d_{s,eq}$	=	equivalent steel effective depth
d_f	=	central distance of FRP bars from top face of section
$D1$	=	steel bar diameter
$D2$	=	steel bar diameter
E	=	tensile modulus of elasticity of FRC
E_c	=	compressive modulus of elasticity of concrete
E_{cr}	=	tensile post cracking modulus of FRC
E_s	=	modulus of elasticity of steel bars
E_f	=	modulus of elasticity of FRP bars
F_f^{pr}	=	Pre-stressing load of FRP bars
F_{Ftuk}	=	characteristic value of the ultimate residual tensile strength of FRC
F_s^{pr}	=	Pre-stressing load of steel bars
F_{pr}	=	Total pre-stressing load
f_{cd}	=	the design value of the concrete compressive strength
f_{ctk}	=	the characteristic value of the tensile strength for the concrete matrix
f_{ck}	=	the characteristic value of cylindrical compressive strength for the concrete matrix
EI	=	flexural stiffness
k	=	the neutral axis depth ratio
k_d	=	factor to take into account the size effect
L	=	beam total length
l_{bd}	=	design anchorage length
L_s		beam span length
M	=	bending moment
$M_i^{'}$	=	normalized bending moment (M / M_{cr}) in stage i
M_i	=	bending moment in stage i
M_{cr}	=	bending moment at FRC crack initiation
M_{mid}		bending moment at beam mid-span
M_s^{pr}	=	bending moment corresponding to pre-stress load of steel bars
M_f^{pr}	=	bending moment corresponding to pre-stress load of FRP bars

ΔM = bending moment increment with respect to non prestressed beam

$M^{pr=25/50}$ = the moment for a pre-stress level of 25% or 50%

$M^{pr=0.0}$ = the moment for non pre-stressed beam

N_{Ed} = axial force due to loading or pre-stressing actions

P = total applied load on beam

P_{fl} = ultimate applied load corresponding to flexural resistance

P_{sh} = ultimate applied load corresponding to shear resistance

ΔP = total applied load increment with respect to non prestressed beam

$P^{pr=25/50}$ = the load for a pre-stress level of 25% or 50%

$P^{pr=0.0}$ = the load for non pre-stressed beam

$\Delta P_{\delta=10\,mm}$ = total applied load increment at δ=10mm for α equal to 10, 50, or 150

$P_{\delta=10\,mm}^{\alpha=1.01}$ = the load at δ=10mm for α=1.01

V_{Rd} = design value of shear resistance

$V_{Rd,F}$ = design shear resistance attributed to the FRC

$V_{Rd,\max}$ = maximum design value of shear resistance

$V_{Rd,s}$ = design shear resistance provided by shear reinforcement

w = width of CFRP laminate

α = normalized transition strain

β = normalized tensile strain at bottom fibre

β_{tu} = normalized ultimate tensile strain

γ = normalized compressive modulus of elasticity of FRC

γ_c = partial safety factor for the concrete material properties

γ_f = normalized modulus of elasticity of FRP bars

γ_F = partial safety factor for FRC

γ_s = normalized modulus of elasticity of steel bars

δ_{mid} = flexural beam deflection at mid-span

ε_{cy} = compressive yield strain of FRC

ε_{cu} = ultimate compressive strain of FRC

ε_{cr} = tensile strain at crack initiation of FRC

ε_{sy} = tensile yield strain of steel bars

ε_{su} = ultimate tensile strain of steel bars

ε_{tm} = tensile strain at transition point of FRC

ε_{tbot} = tensile strain at the bottom of FRC

ε_{ctop} = compressive strain at the top of FRC

ε_{tu} = ultimate tensile strain of FRC

ε_{fu} = ultimate tensile strain of FRP bars

ε_s^{pr} = pre-stressing strain of steel bars

ε_f^{pr} = pre-stressing strain of FRP bars

ζ = normalized transition tensile strain of steel bars

η = normalized post-crack modulus of FRC

λ = normalized compressive strain at the FRC top fibre

λ_{cu} = normalized ultimate compressive strain of FRC

μ = Normalized post-crack residual strength of FRC

ν = normalized tensile strain of FRP bars

ν_{fu} = normalized ultimate tensile strain of FRP bars

ρ_s = reinforcement ratio of longitudinal steel bars

$\rho_{s,eq}$ = equivalent steel reinforcement ratio

ρ_f = reinforcement ratio of longitudinal FRP bars

ρ_l = reinforcement ratio of the longitudinal reinforcement

σ_c = compressive stress of FRC

σ_{cp} = average stress acting on the concrete cross section

σ_{cy} = compressive yield stress of FRC

σ_t = tensile stress of FRC

σ_s = tensile stress of the steel bars

σ_f = tensile stress of the FRP bars

σ_{sy} = tensile yield stress of steel bars

σ_{sr} = the maximum steel stress in a crack in the crack formation stage

σ_{cr} = tensile strength of FRC

σ_{cst} = residual tensile stress of FRC

χ = curvature

χ_{cr} = curvature at crack initiation of FRC

χ_i' = normalized curvature χ / χ_{cr}

χ_i = curvature in stage i

ψ = normalized tensile strain of steel bars

ψ_{su} = normalized ultimate steel tensile strain of steel bars

ω = normalized compressive yield strain of FRC

Δ_s = normalized cover thickness of steel bars

Δ_f = normalized cover thickness of FRP bars

List of Figures:

List of Tables:

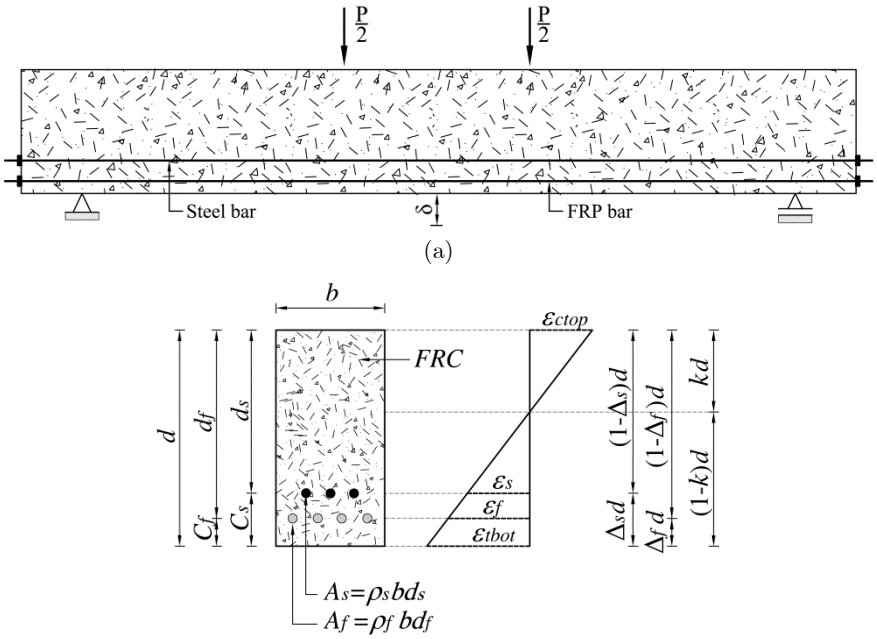

Fig. 1 – (a) Concept of FRC-hybrid reinforcing system, and (b) variables involved in the analytical model.

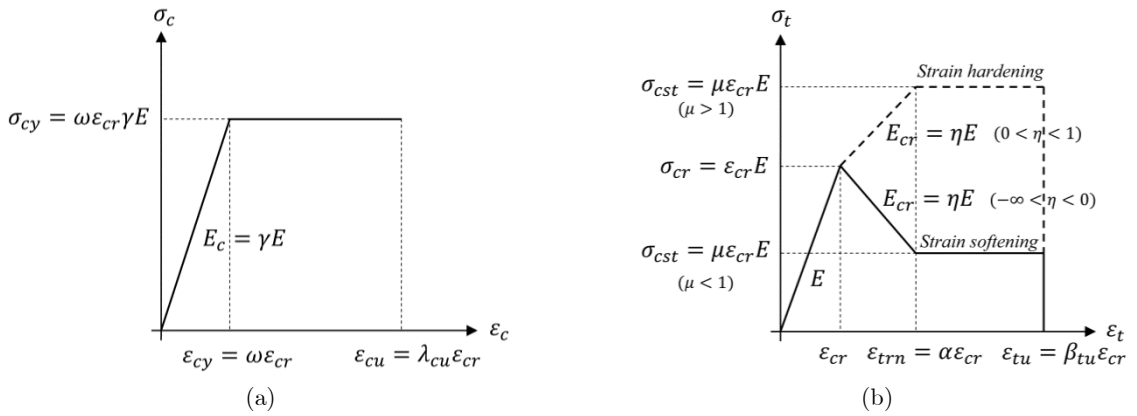

Fig. 2 – Stress-strain diagrams for modelling the: a) compression and b) tensile behaviour of fibre reinforced concrete with softening or hardening character [21].

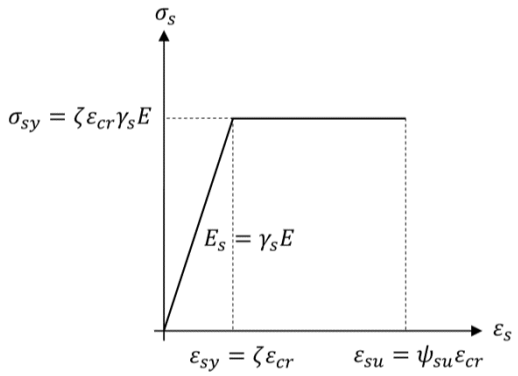

Fig. 3 - Tensile stress-strain relationship for the steel bars.

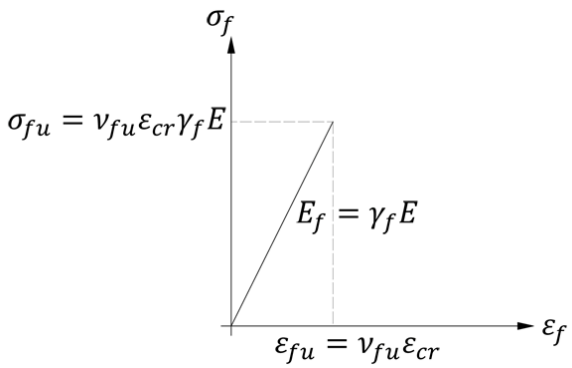

Fig. 4 - Tensile stress-strain relationship for FRP bars.

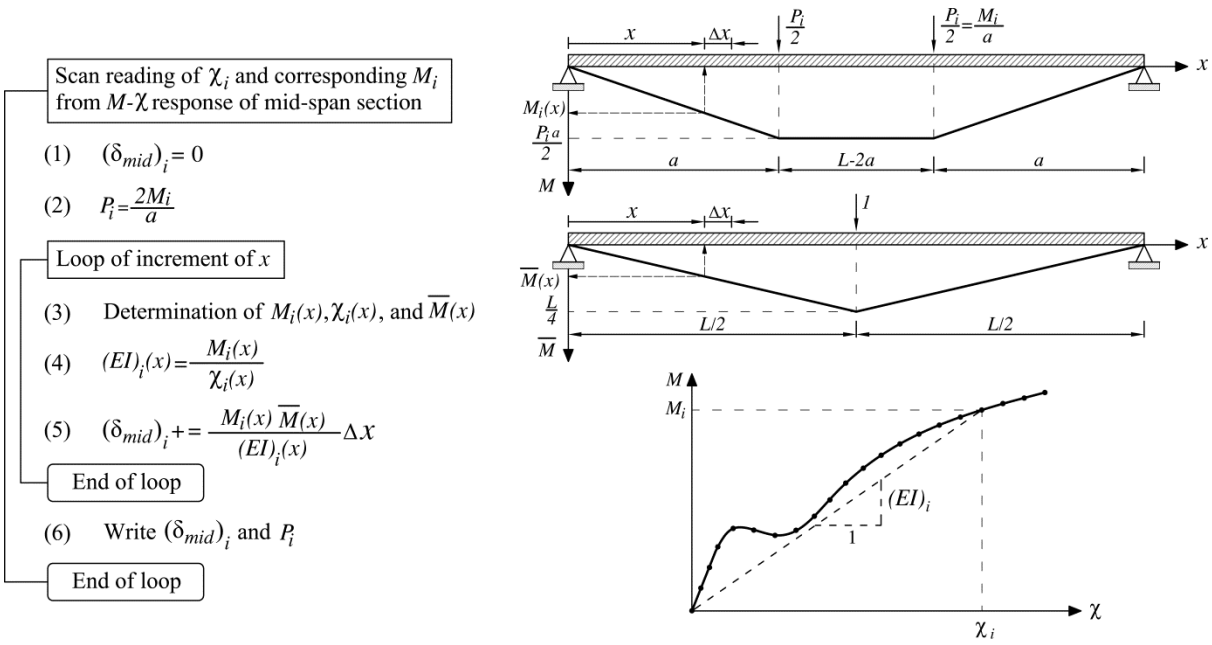

Fig. 5 - Numerical approach to simulate the force-deflection response of simple supported beams failing in bending

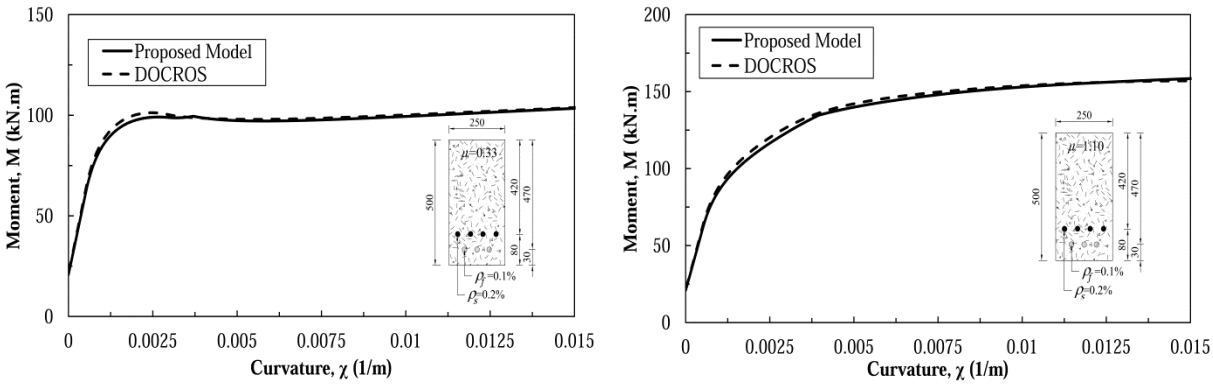

(a) *(b)*

Fig. 6 - Moment-curvature responses predicted by the model and DOCROS software for the cross section of a beam made by: (a) strain softening FRC; (b) strain hardening FRC (the dimensions of the cross section are in mm).

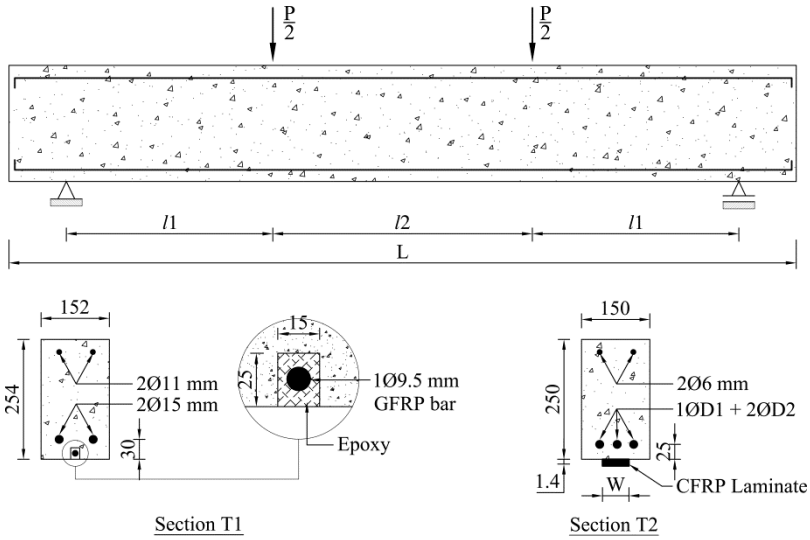

Fig. 7- Geometry of the beams, reinforcement and strengthening configurations (dimensions in mm)

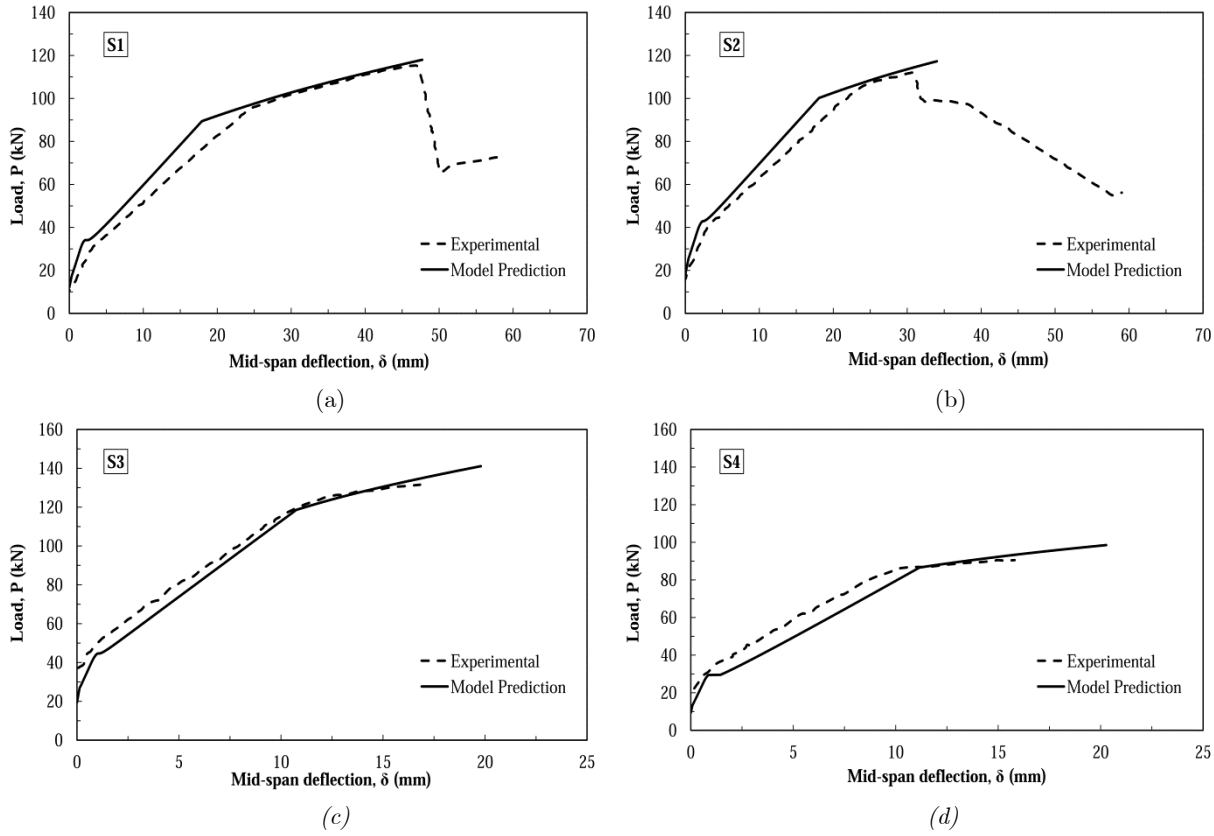

Fig. 8 - Force versus deflection relationship determined from the developed model and registered in the experimental tests for: (a) S1 [24], (b) S2 [24], (c) S3 [25], (d) S4 [25].

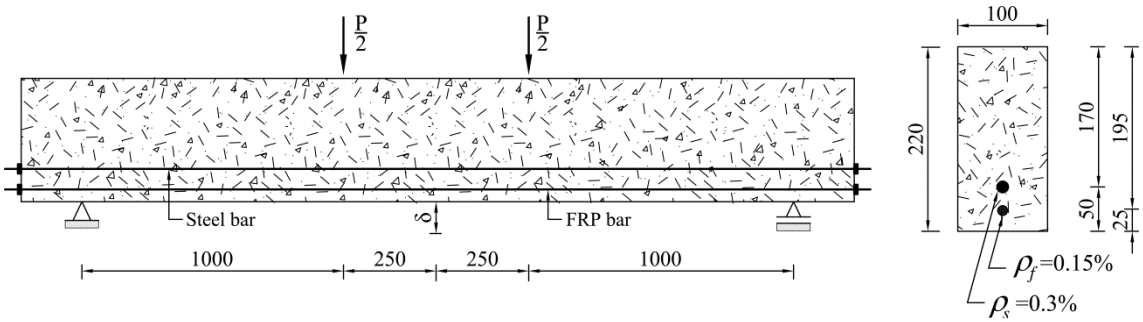

Fig. 9 – Geometry and reinforcement data for the beam of the parametric study (dimensions in mm).

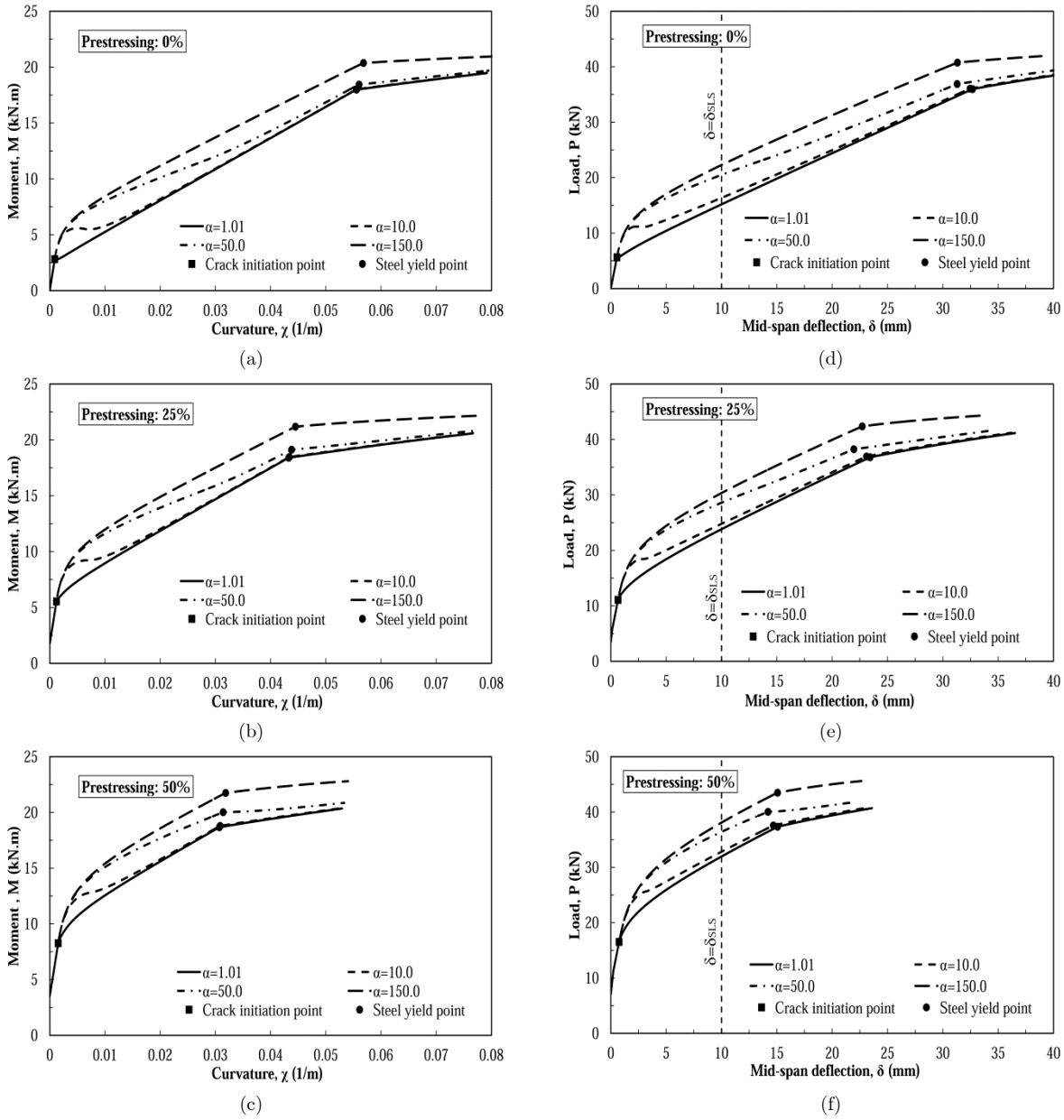

Fig. 10 - Effect of the α parameter on the moment-curvature and load-deflection responses for $\mu = 0.4$, and steel and FRP bars pre-stressed at 0.0, 25, 50%.

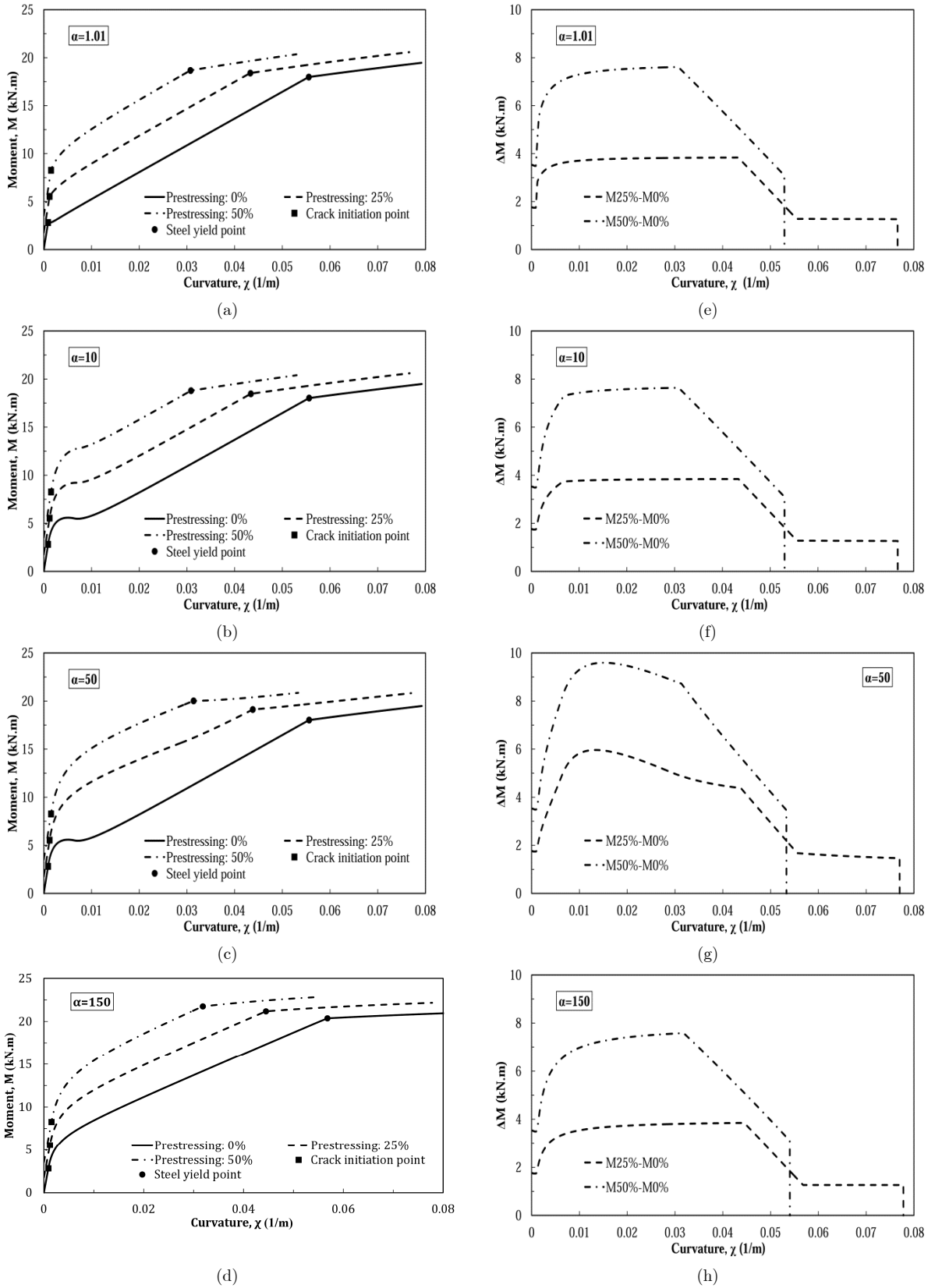

Fig. 11 – Effect of the pre-stress level on the: (a-d) moment-curvature response; (e-h) increase of the resisting bending moment; for $\mu = 0.4$ and α *equal to 1.01, 10.0, 50.0 and 150.0.*

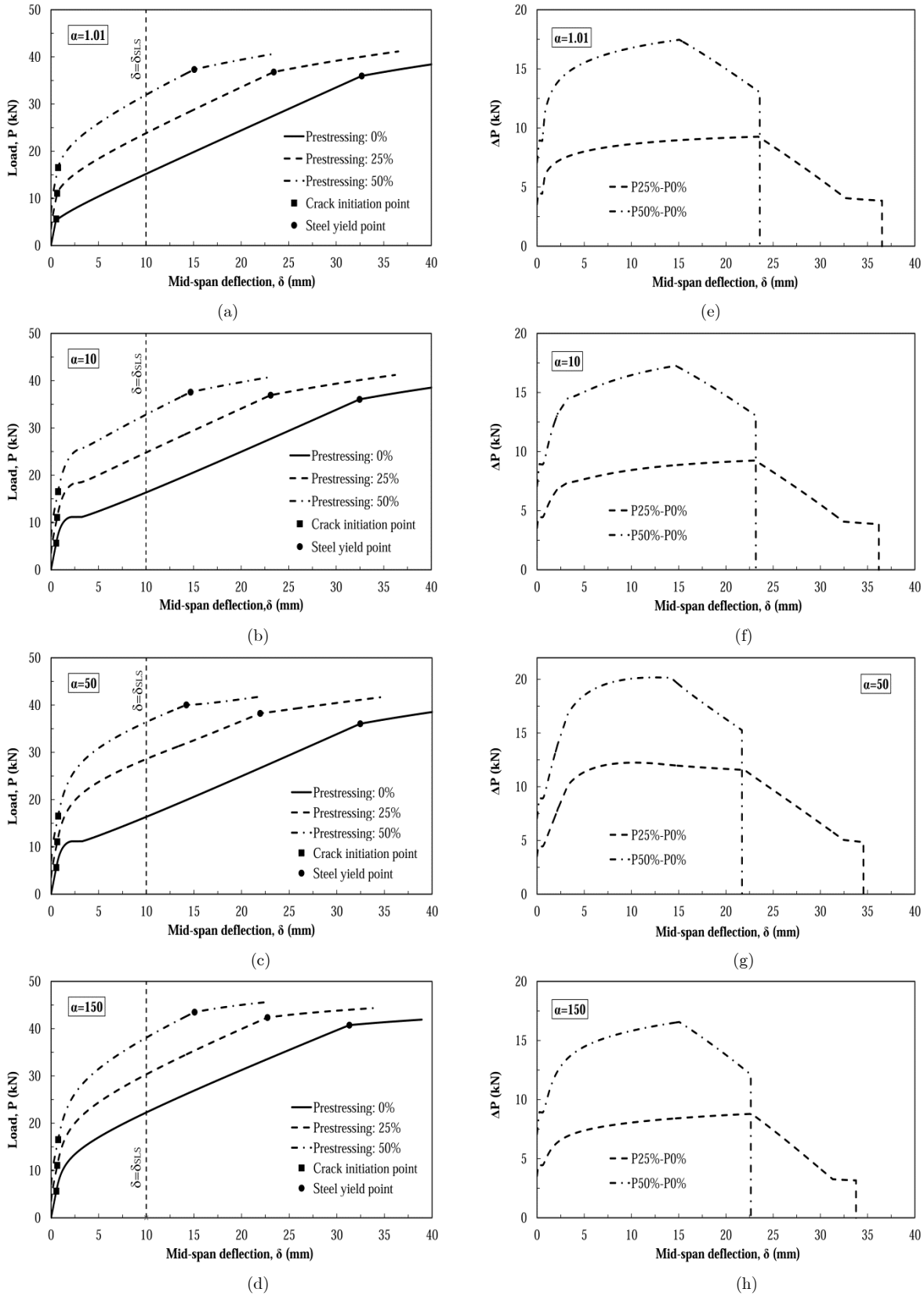

Fig. 12 - Effect of the pre-stress level on the: (a-d) Load-deflection response; (e-h) increase of the load carrying capacity; for $\mu = 0.4$ *and* α *equal to 1.01,10, 50, and 150.*

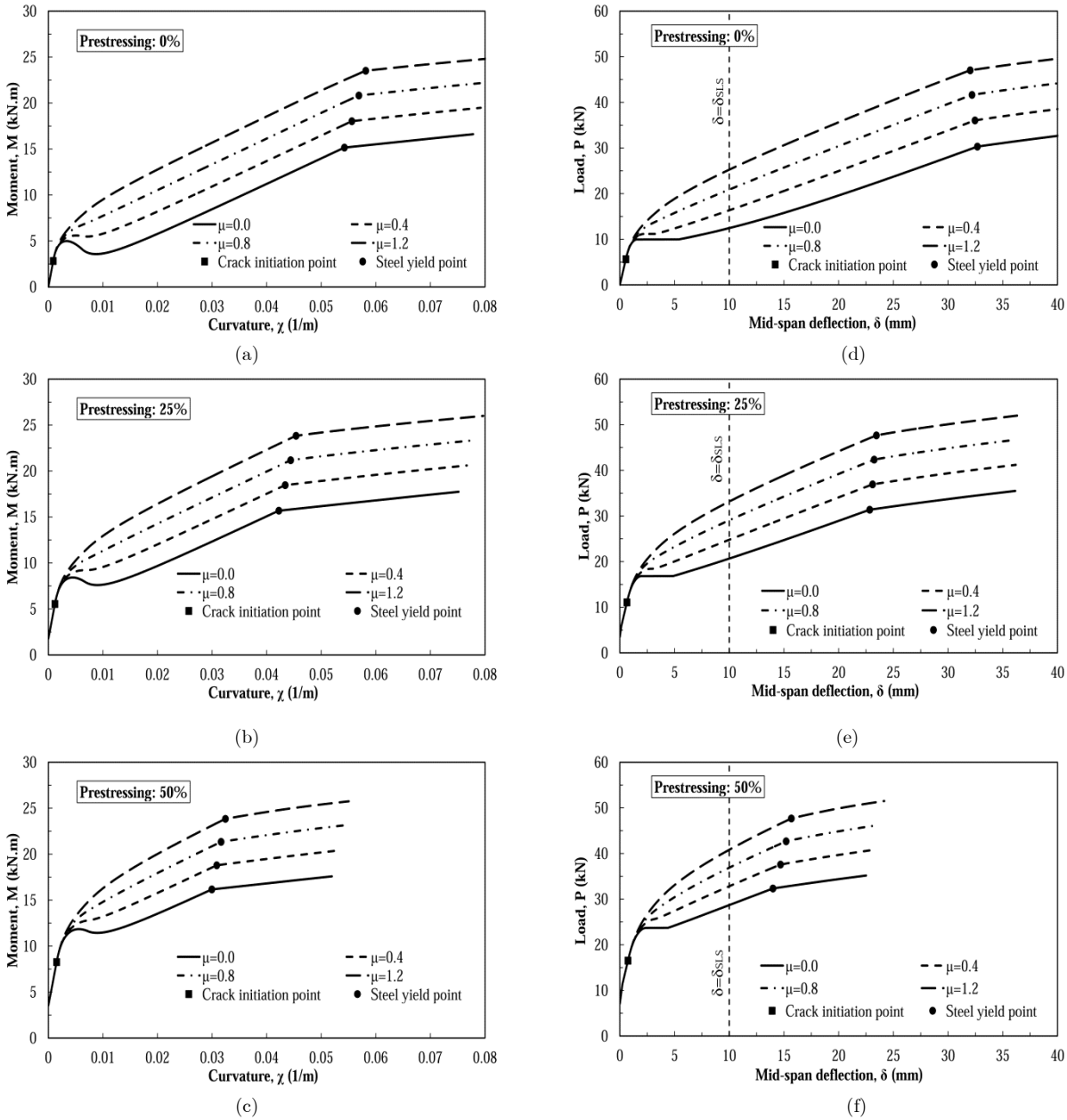

Fig. 13 - Effect of the μ parameter on the moment-curvature and load-deflection responses for $\alpha=10$, and steel and FRP bars pre-stressed at 0.0, 25, 50%.

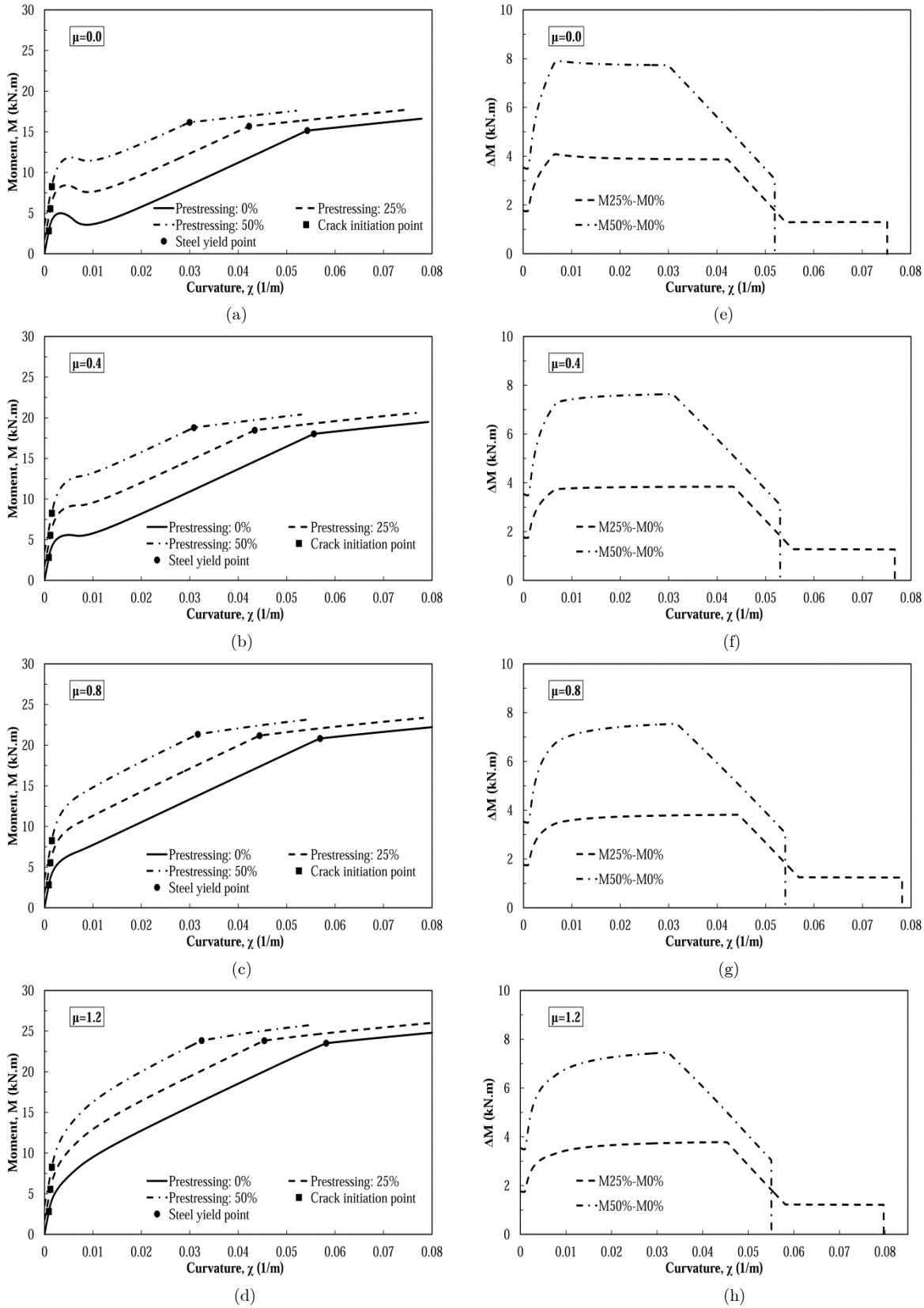

Fig. 14 - Effect of the pre-stress level on the: (a-d) moment-curvature response; (e-h) increase of the resisting bending moment; for $\alpha = 10$ *and* μ *equal to 0.0, 0.4, 0.8, 1.2.*

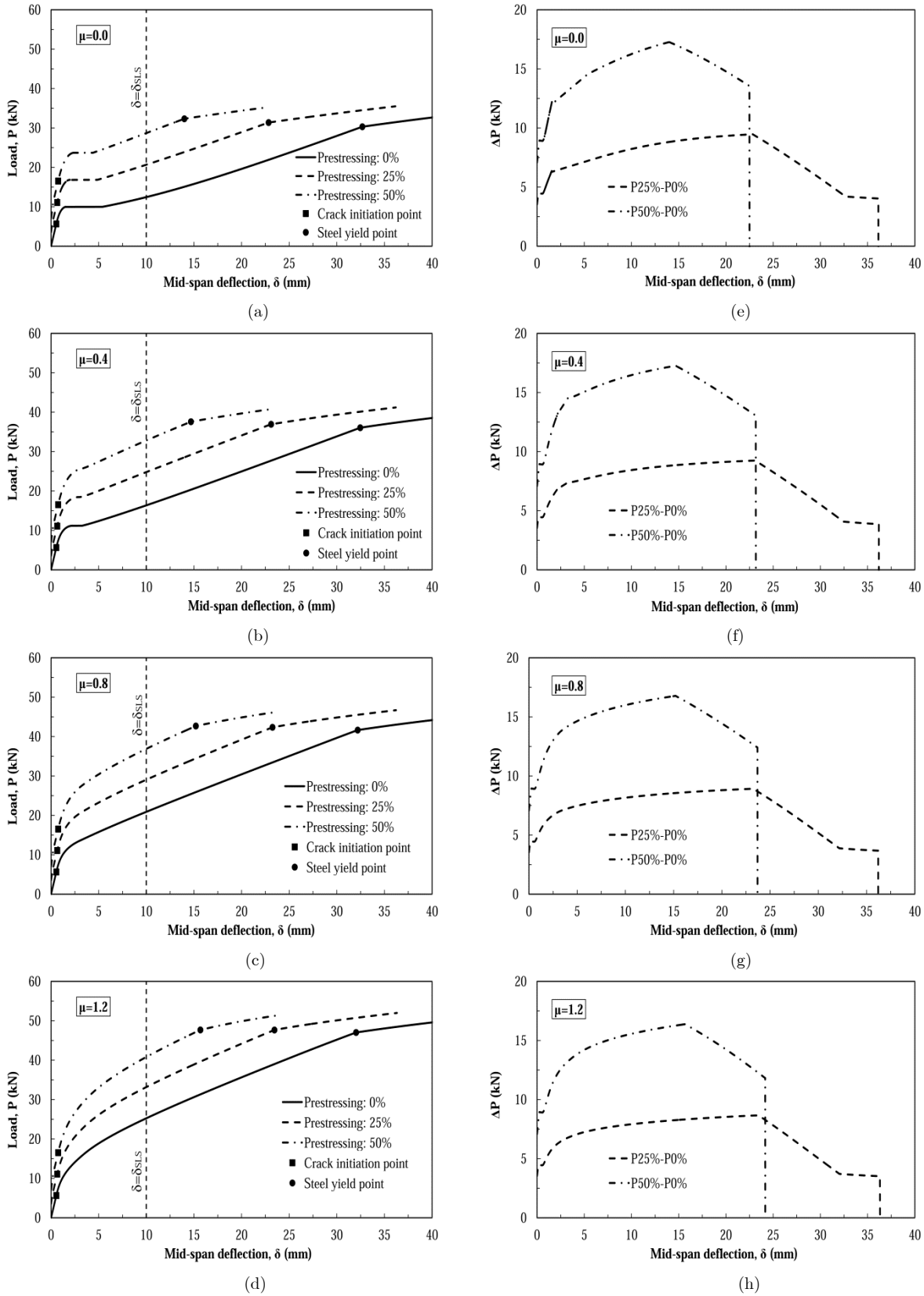

Fig. 15 - Effect of the pre-stress level on the: (a-d) Load-deflection response; (e-h) increase of the load carrying capacity; for $\alpha = 10$ *and* μ *equal to 0.0, 0.4, 0.8, 1.2.*

Table 1 - Variations of normalized strain parameters of the intervening materials in the possible stages.

Stage	*Concrete*		*Steel*	*FRP*
	Tension	*Compression*		
1	$0 < \beta \leq 1$	$0 < \lambda \leq \omega$	$0 < \psi \leq \zeta$	$0 < \nu \leq \nu_{fu}$
2.1.1.1	$1 < \beta \leq \alpha$	$0 < \lambda \leq \omega$	$0 < \psi \leq \zeta$	$0 < \nu \leq \nu_{fu}$
2.1.2.1	$1 < \beta \leq \alpha$	$0 < \lambda \leq \omega$	$\zeta < \psi \leq \psi_{su}$	$0 < \nu \leq \nu_{fu}$
2.2.1.1	$1 < \beta \leq \alpha$	$\omega < \lambda \leq \lambda_{cu}$	$0 < \psi \leq \zeta$	$0 < \nu \leq \nu_{fu}$
2.2.2.1	$1 < \beta \leq \alpha$	$\omega < \lambda \leq \lambda_{cu}$	$\zeta < \psi \leq \psi_{su}$	$0 < \nu \leq \nu_{fu}$
3.1.1.1	$\alpha < \beta \leq \beta_{tu}$	$0 < \lambda \leq \omega$	$0 < \psi \leq \zeta$	$0 < \nu \leq \nu_{fu}$
3.1.2.1	$\alpha < \beta \leq \beta_{tu}$	$0 < \lambda \leq \omega$	$\zeta < \psi \leq \psi_{su}$	$0 < \nu \leq \nu_{fu}$
3.2.1.1	$\alpha < \beta \leq \beta_{tu}$	$\omega < \lambda \leq \lambda_{cu}$	$0 < \psi \leq \zeta$	$0 < \nu \leq \nu_{fu}$
3.2.2.1	$\alpha < \beta \leq \beta_{tu}$	$\omega < \lambda \leq \lambda_{cu}$	$\zeta < \psi \leq \psi_{su}$	$0 < \nu \leq \nu_{fu}$

Table 2 - Equations for the evaluation of the depth of the neutral axis parameter, k, for each stage [22].

Stage	k	
1	$k_1 = \begin{cases} \dfrac{2B_s(1-\Delta_s)+2B_f(1-\Delta_f)+1+(2F_{pr}/\beta)}{2\sqrt{D_1}} & for\ \gamma = 1 \\ \dfrac{-\left(1+B_s+B_f+(F_{pr}/\beta)\right)+\sqrt{D_1}}{(\gamma-1)} & for\ \gamma<1 or\ \gamma>1 \end{cases}$	$D_1 = (B_s+B_f+1+(1/\beta)F_{pr})^2-(1-\gamma)(1+2B_s(1-\Delta_s)+2B_f(1-\Delta_f)+(2/\beta)F_{pr})$
2.1.1.1	$k_{2111} = \dfrac{D_{2111}+\beta(\beta(B_s+B_f)+F_{pr})-\sqrt{(D_{2111}+\beta(\beta(B_s+B_f)+F_{pr}))^2-(D_{2111}-\beta^2\gamma)(D_{2111}+2\beta(\beta(B_s(1-\Delta_s)+B_f(1-\Delta_f))+F_{pr}))}}{D_{2111}-\beta^2\gamma}$	$D_{2111} = \eta(\beta-1)^2+2\beta-1$
2.1.2.1	$k_{2121} = \dfrac{D_{2121}+\beta(\zeta B_s+\beta B_f+F_f^{pr})-\sqrt{(D_{2121}+\beta(\zeta B_s+\beta B_f+F_f^{pr}))^2-(D_{2121}-\beta^2\gamma)(D_{2121}+2\beta(\zeta B_s+\beta B_f(1-\Delta_f)+F_f^{pr}))}}{D_{2121}-\beta^2\gamma}$	$D_{2121} = \eta(\beta-1)^2+2\beta-1$
2.2.1.1	$k_{2211} = \dfrac{D_{2211}+\beta(\omega\gamma+\beta(B_s+B_f)+F_{pr})-\sqrt{(D_{2211}+\beta(\omega\gamma+\beta(B_s+B_f)+F_{pr}))^2-(D_{2211}+2\omega\gamma\beta)(D_{2211}+2\beta(\beta B_s(1-\Delta_s)+\beta B_f(1-\Delta_f)+F_{pr}))}}{D_{2211}+2\omega\gamma\beta}$	$D_{2211} = \eta(\beta-1)^2+2\beta-1+\omega^2\gamma$
2.2.2.1	$k_{2221} = \dfrac{D_{2221}+\beta(\beta B_f+\zeta B_s+\omega\gamma+F_f^{pr})-\sqrt{(D_{2221}+\beta(\beta B_f+\zeta B_s+\omega\gamma+F_f^{pr}))^2-(D_{2221}+2\omega\gamma\beta)(D_{2221}+2\beta(\zeta B_s+\beta B_f(1-\Delta_f)+F_f^{pr}))}}{D_{2221}+2\omega\gamma\beta}$	$D_{2221} = \eta(\beta-1)^2+2\beta-1+\omega^2\gamma$
3.1.1.1	$k_{3111} = \dfrac{D_{3111}+\beta(\beta(B_s+B_f)+F_{pr})-\sqrt{(D_{3111}+\beta(\beta(B_s+B_f)+F_{pr}))^2-(D_{3111}-\beta^2\gamma)(D_{3111}+2\beta(\beta(B_s(1-\Delta_s)+B_f(1-\Delta_f))+F_{pr}))}}{D_{3111}-\beta^2\gamma}$	$D_{3111} = \eta(\alpha-1)^2+2(\alpha(1-\mu)+\mu\beta)-1$
3.1.2.1	$k_{3121} = \dfrac{D_{3121}+\beta(\beta B_f+\zeta B_s+F_f^{pr})-\sqrt{(D_{3121}+\beta(\beta B_f+\zeta B_s+F_f^{pr}))^2-(D_{3121}-\beta^2\gamma)(D_{3121}+2\beta(\zeta B_s+\beta B_f(1-\Delta_f)+F_f^{pr}))}}{D_{3121}-\beta^2\gamma}$	$D_{3121} = \eta(\alpha-1)^2+2(\alpha(1-\mu)+\mu\beta)-1$
3.2.1.1	$k_{3211} = \dfrac{D_{3211}+\beta(\beta(B_s+B_f)+\omega\gamma+F_{pr})-\sqrt{(D_{3211}+\beta(\beta(B_s+B_f)+\omega\gamma+F_{pr}))^2-(D_{3211}+2\omega\gamma\beta)(D_{3211}+2\beta(\beta(B_s(1-\Delta_s)+B_f(1-\Delta_f))+F_{pr}))}}{D_{3211}+2\omega\gamma\beta}$	$D_{3211} = \eta(\alpha-1)^2+2(\alpha(1-\mu)+\mu\beta)+\omega^2\gamma-1$
3.2.2.1	$k_{3221} = \dfrac{D_{3221}+\beta(\zeta B_s+\omega\gamma+F_f^{pr})+\beta^2 B_f-\sqrt{(D_{3221}+\beta(\zeta B_s+\omega\gamma+F_f^{pr})+\beta^2 B_f)^2-(D_{3221}+2\omega\gamma\beta)(D_{3221}+2\beta(\zeta B_s+\beta B_f(1-\Delta_f)+F_f^{pr}))}}{D_{3221}+2\omega\gamma\beta}$	$D_{3221} = \eta(\alpha-1)^2+2(\alpha(1-\mu)+\mu\beta)+\omega^2\gamma-1$

$B_s = \gamma_s \rho_s (1-\Delta_s),\ B_f = \gamma_f \rho_f (1-\Delta_f),\ F_{pr} = F_s^{pr} + F_f^{pr}$

.

Table 3 - Equations for the evaluation of the normalized moment, M', and normalized curvature, χ', for each stage [22].

Stage (i)	M'	χ'
1	$M'_1 = \frac{2\beta\left((\gamma-1)k_1^3 + 3\left(B_s+B_f+1\right)k_1^2 - 6\left(B_s(1-\Delta_s)+B_f(1-\Delta_f)+0.5\right)k_1 + 3\left(B_s(1-\Delta_s)^2 + B_f(1-\Delta_f)^2\right)+1\right)}{(1-k_1)} + \left(M'_{pr}\right)_1$ $\left(M'_{pr}\right)_1 = 6F_s^{pr}(1-k_1-\Delta_s) + 6F_f^{pr}(1-k_1-\Delta_f)$	$\chi'_1 = \frac{\beta}{2(1-k_1)}$
2.1.1.1	$M'_{2111} = \frac{(2\beta\gamma + C_{2111})k_{2111}^3 + 3(\beta B_s + \beta B_f - 0.5C_{2111})k_{2111}^2 + 12\left(0.25C_{2111} - \beta\left(B_s(1-\Delta_s)+B_f(1-\Delta_f)\right)\right)k_{2111} + 6\beta\left(B_s(1-\Delta_s)^2 + B_f(1-\Delta_f)^2\right) - C_{2111}}{(1-k_{2111})} + \left(M'_{pr}\right)_{2111}$ $C_{2111} = \frac{-2\eta\beta^3 + 3\beta^2(\eta-1) - \eta + 1}{\beta^2}$, $\left(M'_{pr}\right)_{2111} = 6F_s^{pr}(1-k_{2111}-\Delta_s) + 6F_f^{pr}(1-k_{2111}-\Delta_f)$	$\chi'_{2111} = \frac{\beta}{2(1-k_{2111})}$
2.1.2.1	$M'_{2121} = \frac{(2\beta\gamma + C_{2121})k_{2121}^3 + 6(\zeta B_s + \beta B_f - 0.5C_{2121})k_{2121}^2 + 12\left(0.25C_{2121} + 0.5\zeta B_s(\Delta_s-2) - \beta B_f(1-\Delta_f)\right)k_{2121} + 6\left(\zeta B_s(1-\Delta_s) + \beta B_f(1-\Delta_f)^2\right) - C_{2121}}{(1-k_{2121})} + \left(M'_{pr}\right)_{2121}$ $C_{2121} = \frac{-2\eta\beta^3 + 3\beta^2(\eta-1) - \eta + 1}{\beta^2}$, $\left(M'_{pr}\right)_{2121} = 6F_f^{pr}(1-k_{2121}-\Delta_f)$	$\chi'_{2121} = \frac{\beta}{2(1-k_{2121})}$
2.2.1.1	$M'_{2211} = \frac{-(3\omega\gamma + C_{2211})k_{2211}^3 + 3(\omega\gamma + C_{2211} + 2\beta B_s + 2\beta B_f)k_{2211}^2 - 12\left(0.25C_{2211} + \beta\left(B_s(1-\Delta_s)+B_f(1-\Delta_f)\right)\right)k_{2211} + 6\left(\beta B_s(1-\Delta_s)^2 + \beta B_f(1-\Delta_f)^2\right) + C_{2211}}{(1-k_{2211})} + \left(M'_{pr}\right)_{2211}$ $C_{2211} = \frac{2\eta\beta^3 + 3\beta^2(1-\eta) - \omega^3\gamma + \eta - 1}{\beta^2}$, $\left(M'_{pr}\right)_{2211} = 6F_s^{pr}(1-k_{2211}-\Delta_s) + 6F_f^{pr}(1-k_{2211}-\Delta_f)$	$\chi'_{2211} = \frac{\beta}{2(1-k_{2211})}$
2.2.2.1	$M'_{2221} = \frac{-(3\omega\gamma + C_{2221})k_{2221}^3 + 6\left(0.5(\omega\gamma + 3C_{2221}) + \zeta B_s + \beta B_f\right)k_{2221}^2 - 12\left(0.25C_{2221} + \zeta B_s(1-0.5\Delta_s) - \beta B_f(1-\Delta_f)\right)k_{2221} + 6\left(\zeta B_s(1-\Delta_S) + \beta B_f(1-\Delta_f)^2\right) + C_{2221}}{(1-k_{2221})} + \left(M'_{pr}\right)_{2221}$ $C_{2221} = \frac{2\eta\beta^3 + 3\beta^2(1-\eta) - \omega^3\gamma + \eta - 1}{\beta^2}$, $\left(M'_{pr}\right)_{2221} = 6F_f^{pr}(1-k_{2221}-\Delta_f)$	$\chi'_{2221} = \frac{\beta}{2(1-k_{2221})}$
3.1.1.1	$M'_{3111} = \frac{(C_{3111} - 2\beta\gamma)k_{3111}^3 - 3(2\beta B_s + 2\beta B_f + C_{3111})k_{3111}^2 + 12\left(0.25C_{3111} + \beta\left(B_s(1-\Delta_s)+B_f(1-\Delta_f)\right)\right)k_{3111} - 6\beta\left(B_s(1-\Delta_s)^2 + B_f(1-\Delta_f)^2\right) - C_{3111}}{(k_{3111}-1)} + \left(M'_{pr}\right)_{3111}$ $C_{3111} = \frac{3\left(\mu\beta^2 + \alpha^2(1-\mu-\eta)\right) + \eta\left(2\alpha^3+1\right) - 1}{\beta^2}$, $\left(M'_{pr}\right)_{3111} = 6F_s^{pr}(1-k_{3111}-\Delta_s) + 6F_f^{pr}(1-k_{3111}-\Delta_f)$	$\chi'_{3111} = \frac{\beta}{2(1-k_{3111})}$
3.1.2.1	$M'_{3121} = \frac{(C_{3121} - 2\beta\gamma)k_{3121}^3 - 6(\zeta B_s + \beta B_f + 0.5C_{3121})k_{3121}^2 + 12\left(0.25C_{3121} + 0.5\zeta B_s(2-\Delta_s) + \beta B_f(1-\Delta_f)\right)k_{3121} - 6\left(\zeta B_s(1-\Delta_s) + \beta B_f(1-\Delta_f)^2\right) - C_{3121}}{(k_{3121}-1)} + \left(M'_{pr}\right)_{3121}$ $C_{3111} = \frac{3\left(\mu\beta^2 + \alpha^2(1-\mu-\eta)\right) + \eta\left(2\alpha^3+1\right) - 1}{\beta^2}$, $\left(M'_{pr}\right)_{3121} = 6F_f^{pr}(1-k_{3121}-\Delta_f)$	$\chi'_{3121} = \frac{\beta}{2(1-k_{3121})}$
3.2.1.1	$M'_{3211} = \frac{-(3\omega\gamma + C_{3211})k_{3211}^3 + 6\left(0.5(\omega\gamma + C_{3211}) + \beta(B_s+B_f)\right)k_{3211}^2 - 12\left(0.25C_{3211} + \beta\left(B_s(1-\Delta_s)+B_f(1-\Delta_f)\right)\right)k_{3211} + 6\beta\left(B_s(1-\Delta_s)^2 + B_f(1-\Delta_f)^2\right) + C_{3211}}{(1-k_{3211})} + \left(M'_{pr}\right)_{3211}$ $C_{3211} = \frac{3\left(\mu\beta^2 + \alpha^2(1-\mu-\eta)\right) + \eta\left(2\alpha^3+1\right) - \omega^3\gamma - 1}{\beta^2}$, $\left(M'_{pr}\right)_{3211} = 6F_s^{pr}(1-k_{3211}-\Delta_s) + 6F_f^{pr}(1-k_{3211}-\Delta_f)$	$\chi'_{3211} = \frac{\beta}{2(1-k_{3211})}$
3.2.2.1	$M'_{3221} = \frac{-(3\omega\gamma + C_{3221})k_{3221}^3 + 6\left(0.5(\omega\gamma + C_{3221}) + (\zeta B_s + \beta B_f)\right)k_{3221}^2 - 12\left(0.25C_{3221} + 0.5\zeta B_s(2-\Delta_s) + \beta B_f(\Delta_f - 1)\right)k_{3221} + 6\left(\zeta B_s(1-\Delta_s) + \beta B_f(1-\Delta_f)^2\right) + C_{3221}}{(1-k_{3221})} + \left(M'_{pr}\right)_{3221}$	$\chi'_{3221} = \frac{\beta}{2(1-k_{3221})}$

$$C_{3211}=\frac{3\left(\mu\beta^{2}+\alpha^{2}\left(1-\mu-\eta\right)\right)+\eta\left(2\alpha^{3}+1\right)-\omega^{3}\gamma-1}{\beta^{2}}\quad,\qquad \left(M_{pr}^{'}\right)_{3221}=6F_{f}^{pr}\left(1-k_{3221}-\Delta_{f}\right)$$

$$B_{s}=\gamma_{s}\rho_{s}\left(1-\Delta_{s}\right),\ B_{f}=\gamma_{f}\rho_{f}\left(1-\Delta_{f}\right),\ F_{pr}=F_{s}^{pr}+F_{f}^{pr}$$

.

Table 4 - Data for the model parameters used in the examples for the assessment of the predictive performance of the developed model.

Geometric parameters (mm)		*Mechanical parameters*												
		Concrete (tension)					*Concrete (compression)*			*Steel (tension)*			*FRP (tension)*	
b	*250*	ε_{cr}	E	α	β_{tu}	μ	ω	γ	λ_{cu}	ζ	γ_s	ψ_{su}	ν_{fu}	γ_f
d	*500*	*(‰)*	*(GPa)*											
C_s	*80*	*0.1*	*30*	*10*	*150*	*1.1 (SH-FRC)* *0.33 (SS-FRC)*	*10*	*1*	*40*	*20*	*6.67*	*120*	*300*	*1*
C_f	*30*													

Table 5 – Data to define the geometry, the reinforcement and the strengthening systems of the beams represented in Fig. 7.

Specimen's designation	*Ref.*	*L (mm)*	*l1 (mm)*	*l2 (mm)*	*Sec. Type*	*W (mm)*	*D1 (mm)*	*D2 (mm)*	*Pre-stressing (%)*
S1	*[24]*	*3500*	*1100*	*1100*	*T1*	-	-	-	*40.0*
S2	*[24]*	*3500*	*1100*	*1100*	*T1*	-	-	-	*60.0*
S3	*[25]*	*2700*	*950*	*600*	*T2*	*50*	*12*	*14*	*42.1*
S4	*[25]*	*2700*	*950*	*600*	*T2*	*20*	*12*	*12*	*50.6*

Table 6 – Data to define the constitutive laws of the intervenient materials in the beams of Fig. 7

Specimen's designation	*Ref.*	σ_{cy} *(MPa)*	σ_{cr} *(MPa)*	E_c *(GPa)*	σ_{sy} *(MPa)*	E_s *(GPa)*	σ_{fu} *(MPa)*	E_f *(GPa)*
S1	*[24]*	*53*	*3.79*	*30.20*	*440*	*190*	*1970*	*136*
S2	*[24]*	*53*	*3.79*	*30.20*	*440*	*190*	*1970*	*136*
S3	*[25]*	*50.3*	*3.60*	*32.50*	*383*	*142*	*2500*	*150*
S4	*[25]*	*50.3*	*3.60*	*32.50*	*429*	*145*	*2500*	*150*

Table 7 - Values considered for the constitutive parameters for the simulation of the series of beams

Specimen's designation	ε_{cr} (‰)	α	μ	β_{tu}	γ	ω	λ_{cu}	ρ_s (%)	γ_s	ζ	ψ_{su}	ρ_f (%)	γ_f	ν_{fu}	ε_s^{pr} (%)	ε_f^{pr} (%)
S1	*0.125*	*2*	*1e-8*	*150*	*1*	*13.98*	*28*	*1.04*	*6.29*	*18.53*	*120*	*0.2082*	*4.50*	*116*	*0.0*	*0.56*
S2	*0.125*	*2*	*1e-8*	*150*	*1*	*13.98*	*28*	*1.04*	*6.29*	*18.53*	*120*	*0.183*	*4.50*	*116*	*0.0*	*0.84*
S3	*0.111*	*2*	*1e-8*	*150*	*1*	*13.97*	*32*	*1.25*	*4.36*	*24.41*	*120*	*0.187*	*4.62*	*150*	*0.0*	*0.70*
S4	*0.111*	*2*	*1e-8*	*150*	*1*	*13.97*	*32*	*1.01*	*4.46*	*26.71*	*120*	*0.075*	*4.62*	*150*	*0.0*	*0.84*

Table 8 - Values for the parameters of the materials constitutive laws adopted in the parametric study

Geometric parameters (mm)		*Mechanical parameters*												
		Concrete (tension)					*Concrete (compression)*			*Steel (tension)*			*GFRP (tension)*	
b	*100*	ε_{cr}	E	α	μ	β_{tu}	ω	γ	λ_{cu}	ζ	γ_s	ψ_{su}	ν_{fu}	γ_f
d	*220*	*(‰)*	*(GPa)*											
C_s	*50*	*0.1*	*35*	[1.01, 10, 50, 150]	0.4	*150*	*20*	*1*	*35*	*75*	*5.71*	*150*	*166.7*	*1.71*
C_f	*25*			10	[0.0, 0.4, 0.8, 1.2]									

Table 9 – Flexural versus shear resistance of hybrid reinforced FRC beams

Pre-stress level (%)	μ	P_{sh} *(kN)*	P_{fl} *(kN)*	Failure mode
0	*0*	*27.58*	*33.22*	*Shear*
	0.4	*43.78*	*38.97*	*Flexure*
	0.8	*52.76*	*44.50*	*Flexure*
	1.2	*59.42*	*49.82*	*Flexure*
25	*0*	*33.84*	*35.49*	*Shear*
	0.4	*50.05*	*41.20*	*Flexure*
	0.8	*59.02*	*46.70*	*Flexure*
	1.2	*65.69*	*51.99*	*Flexure*
50	*0*	*40.10*	*35.18*	*Flexure*
	0.4	*56.31*	*40.80*	*Flexure*
	0.8	*65.29*	*46.25*	*Flexure*
	1.2	*71.95*	*51.51*	*Flexure*